Geochemistry, Geophysics, Geosystems®

AGU ADVANCING EARTH AND SPACE SCIENCES

RESEARCH ARTICLE
10.1029/2025GC012278

Offshore Record of Explosive Volcanic Eruptions in the Southern Part of the Panamá Basin During the Past 10 Myr: 2. Inferences About the Construction of the Northern Andean Arc and Regional Geodynamics

Mathilde Bablon[1], Pablo Samaniego[2], Jean-Luc Le Pennec[3], François Nauret[2], François Michaud[4], Marianne Saillard[1], Silvana Hidalgo[5], Jean-Luc Devidal[2], François Orange[6], Céline Liorzou[7], and Gueorgui Ratzov[1]

[1]Université Côte d'Azur, IRD, CNRS, Observatoire de la Côte d'Azur, Valbonne, France, [2]Université Clermont Auvergne, CNRS, IRD, OPGC, Laboratoire Magmas et Volcans, Clermont-Ferrand, France, [3]Geo-Ocean, University Brest, CNRS, Ifremer, UMR6538, IRD, IUEM, Plouzané, France, [4]Université Côte d'Azur, Sorbonne Universités, CNRS, Observatoire de la Côte d'Azur, IRD, Géoazur, France, [5]Instituto Geofísico, Escuela Politécnica Nacional, Quito, Ecuador, [6]Université Côte d'Azur, Centre Commun de Microscopie Appliquée, Nice, France, [7]Geo-Ocean, University Brest, CNRS, Ifremer, UMR6538, Plouzané, France

Abstract Volcanic material preserved in marine and lacustrine sediments is a key high-resolution archive for studying the past eruptive history of volcanic regions. In this work, we use the geochemical and isotopic compositions of marine volcanic glass shards, the thicknesses, and age models of tephra layers preserved in the deep sediments of the eastern equatorial Pacific, to study their volcanic source, the long-term evolution of volcanism, and its relationship with the regional geodynamics. We highlight that explosive eruptions associated with the Galápagos hotspot occurred in the Late Miocene and Early Pleistocene, which may reflect plume-ridge interplays. We also show that the oldest products of the Northern Andean arc were deposited at ∼4.8 Ma, shortly before the extinction of volcanic activity in northern Peru-southern Ecuador, due to the gradual flattening of the slab. The eruptive activity, apparently restricted to the Eastern Cordillera of Ecuador during the Pliocene, intensified and expanded from 2 Ma, with products of more varied compositions reflecting the construction of stratovolcanoes. This increase in volcanic activity, coeval with episodes of uplift of the Coastal Cordillera and with the development of the regional fault system that accommodates crustal deformations, may reflect the presence under the Ecuadorian Andes of the young Nazca oceanic crust, which carries the Carnegie Ridge. Finally, our results suggest that tephra of the Northern Andean arc recorded in sediments of the Panamá Basin were essentially emplaced by Plinian eruptions of a VEI-5-6 (Volcanic Explosivity Index), except one VEI-7 caldera-forming eruption, which occurred at 216 ± 5 ka.

Plain Language Summary Numerous layers of volcanic ash emitted during the past ∼10 Myr are archived in deep sediments of the eastern equatorial Pacific Ocean. In this work, we use the geochemical signatures of these tephra layers to investigate the long-term evolution of volcanic activity. Most of them are related to the Northern Andean arc. Pliocene rhyolitic tephra have a signature close to products of the Eastern Cordillera in Ecuador, and may correspond to the early construction phase of the current arc. From ∼2 Ma, the number of tephra records increases considerably and their composition becomes more heterogeneous with andesitic and dacitic glass compositions, reflecting the geographical development of the arc, and the construction of stratovolcanoes. This increase in volcanic activity coincides with regional geodynamic changes, including the subduction of the Carnegie Ridge and the development of crustal fault systems. Although many Ecuadorian volcanoes have been studied during the past decades, few distal tephra can be reliably correlated with proximal volcanic products. Our study therefore highlights the importance of combining work in the cordillera and in the marine and lacustrine sedimentary archives to refine the catalog of major regional eruptions and improve knowledge of the past history of the Northern Andean arc.

Key Points:

- 27 tephra layers recorded in deep-sea sediments off Ecuador were emplaced during VEI 5 to 7 eruptions in the Northern Andean arc
- Pliocene tephra layers display rhyolitic compositions with signatures close to those of products from the Eastern Cordillera of Ecuador
- More heterogeneous magma compositions since 2 Ma coincide with the construction of stratovolcanoes and regional geodynamic changes

Supporting Information:

Supporting Information may be found in the online version of this article.

Correspondence to:

M. Bablon,
mathilde.bablon@geoazur.unice.fr

Citation:

Bablon, M., Samaniego, P., Le Pennec, J.-L., Nauret, F., Michaud, F., Saillard, M., et al. (2025). Offshore record of explosive volcanic eruptions in the southern part of the Panamá Basin during the past 10 Myr: 2. Inferences about the construction of the Northern Andean arc and regional geodynamics. *Geochemistry, Geophysics, Geosystems*, *26*, e2025GC012278. https://doi.org/10.1029/2025GC012278

Received 9 MAR 2025
Accepted 31 MAY 2025

Author Contributions:

Conceptualization: Mathilde Bablon
Funding acquisition: Mathilde Bablon, François Michaud, Marianne Saillard, Gueorgui Ratzov
Investigation: Mathilde Bablon, Pablo Samaniego, François Nauret, Jean-Luc Devidal, François Orange, Céline Liorzou
Methodology: Mathilde Bablon
Supervision: Mathilde Bablon

1. Introduction

The volcanic activity of the Northern Andean arc is related to the subduction of the oceanic Nazca plate beneath the South-American plate (Figure 1a). The current volcanic arc extends from 6°N to 2°S. It forms a single row in

Writing – original draft: Mathilde Bablon
Writing – review & editing: Mathilde Bablon, Pablo Samaniego, Jean-Luc Le Pennec, François Nauret, François Michaud, Marianne Saillard, Silvana Hidalgo, Jean-Luc Devidal, François Orange, Céline Liorzou

the Colombian Andes (Figure 1c), and widens significantly in Ecuador, where volcanoes are spread over the Western and Eastern Cordillera, the Interandean Valley, and the Sub-Andean zone (Figure 1b). In Colombia, the older subaerial explosive activity is evidenced by ignimbrites emplaced between 12 and 2 Ma (e.g., Alvarez Silva, 2022; Bernet et al., 2020; Torres Hernández, 2010; Van der Wiel, 1991). The stratovolcanoes of the current volcanic arc are constructed upon the ignimbrites, but the timing of their construction stages is still poorly known. Further south in Ecuador, extensive volcanological investigations conducted over the past 30 years have thoroughly documented the eruptive history and the magma chemistry of numerous eruptive centers (e.g., Bablon, Quidelleur, Samaniego, et al., 2020; Barberi et al., 1988; Hall & Beate, 1991; Hall et al., 2008; Santamaría et al., 2023; and many others). The construction of the oldest stratovolcanoes started between 1.4 and 1.1 Ma in the region of Quito (Samaniego et al., 2005; Hidalgo, 2006; Robin et al., 2010; Santamaría et al., 2024; Figure 1b), and the volcanism intensified from ∼600 ka, associated with an extension of the arc to the north and south (e.g., Bablon et al., 2019; Santamaría et al., 2023; Figure 1b). The oldest volcanic products of the current arc correspond to the activity of the Chacana caldera (up to ∼2.7 Ma; Opdyke et al., 2006), located in the Eastern Cordillera east of Quito (#20; Figure 1b). However, given the tropical climate of the Andes and the high number of volcanoes, several volcanic products may have been eroded or concealed below younger products. It is therefore difficult to get a comprehensive view on land of the early development of the arc, although its study is essential to decipher the long-term evolution of magmatism, the current eruptive dynamics, and the relative geodynamic framework.

In the companion paper (Bablon et al., 2025b), we investigate tephra layers recorded within marine sedimentary sequences in the southern part of the Panamá Basin (DSDP and ODP Sites 504, 677, 678, 1238, 1239 and 1240; Figure 1a). Detailed description and analyses of lithology, mineralogy, morphology of glass shards, major and trace elements compositions, and Sr-Pb isotopic ratios allow us to correlate key tephra beds between drilling sites, and to establish a catalog of major eruptions that occurred in this region since the Late Miocene. In particular, we show that marine sediments recorded volcanic products of at least 27 large explosive eruptions from the Northern Andes for the past 4.8 Ma. Four of them occurred during the Early Pliocene, two during the Late Pliocene, and 21 during the Pleistocene, with a gradual widening of the magma compositional range (i.e., from high-K rhyolitic compositions for Pliocene products to andesitic, dacitic and rhyolitic composition of medium- and high-K magmatic series for Pleistocene products). This suggests that the current arc is not only Quaternary as previously stated (e.g., Bablon, Quidelleur, Samaniego, et al., 2020; Hall & Wood, 1985; Santamaría et al., 2024), but started to develop at least since the Early Pliocene. We also identified two tephra layers in 8.9 ± 0.5 and 4.7 ± 0.3 Ma sediments, whose composition is close to that of products of the Central Andean arc. In addition, at least five tephra layers result from eruptions from the Galápagos hotspot activity between the Late Miocene and the Early Pleistocene, revealing that substantial explosive subaerial eruptions occurred in the Galápagos archipelago at least until 1.36 ± 0.05 Ma.

In this paper, we compare the major and trace elements contents and Sr-Pb isotopic ratios of distal tephra layers with the geochemical composition of Plio-Quaternary products of the Northern Andean arc and the surrounding areas (i.e., the Mio-Pliocene eruptive products of the Peruvian arc and the Galápagos hotspot) to investigate the volcanic source of major explosive eruptions whose products reached the Pacific Ocean. Based on the age models of these eruptions and the compositional evolution of magmas, we discuss the relationship between the development of the Northern Andean arc and the changes in the regional geodynamics since the Late Miocene, with emphasis on the impact of the subduction of an aseismic ridge on volcanism.

2. Geological Context

2.1. Orogeny, Geodynamics and Tectonics of the Northern Andes

The Northern Andes are the result of the ongoing subduction of the oceanic Nazca plate beneath the South American plate (Figure 1a). From a single range in southern Ecuador, the Andes are split into two ranges separated by the Interandean Valley in central and northern Ecuador (Figure 1b), and into three ranges separated by the Cauca-Patía and Magdalena Valleys in Colombia further north (Figure 1c). In Colombia, the uplift of the Central and Western Cordilleras started as early as ∼138 Ma, whereas the exhumation of Ecuadorian Andes occurred later, at ∼85 and 65 Ma for the Western and Eastern Cordilleras, respectively (Spikings et al., 2001, 2005; Villagómez & Spikings, 2013). Regional pulses of exhumation occurred at ∼75–65, ∼45–30, ∼15–13 and ∼9 Ma, synchronously with major geodynamical events (i.e., change in plate kinematics and convergence rates, collision and accretion of oceanic terranes, then collision of the Carnegie Ridge to the margin and the increase of

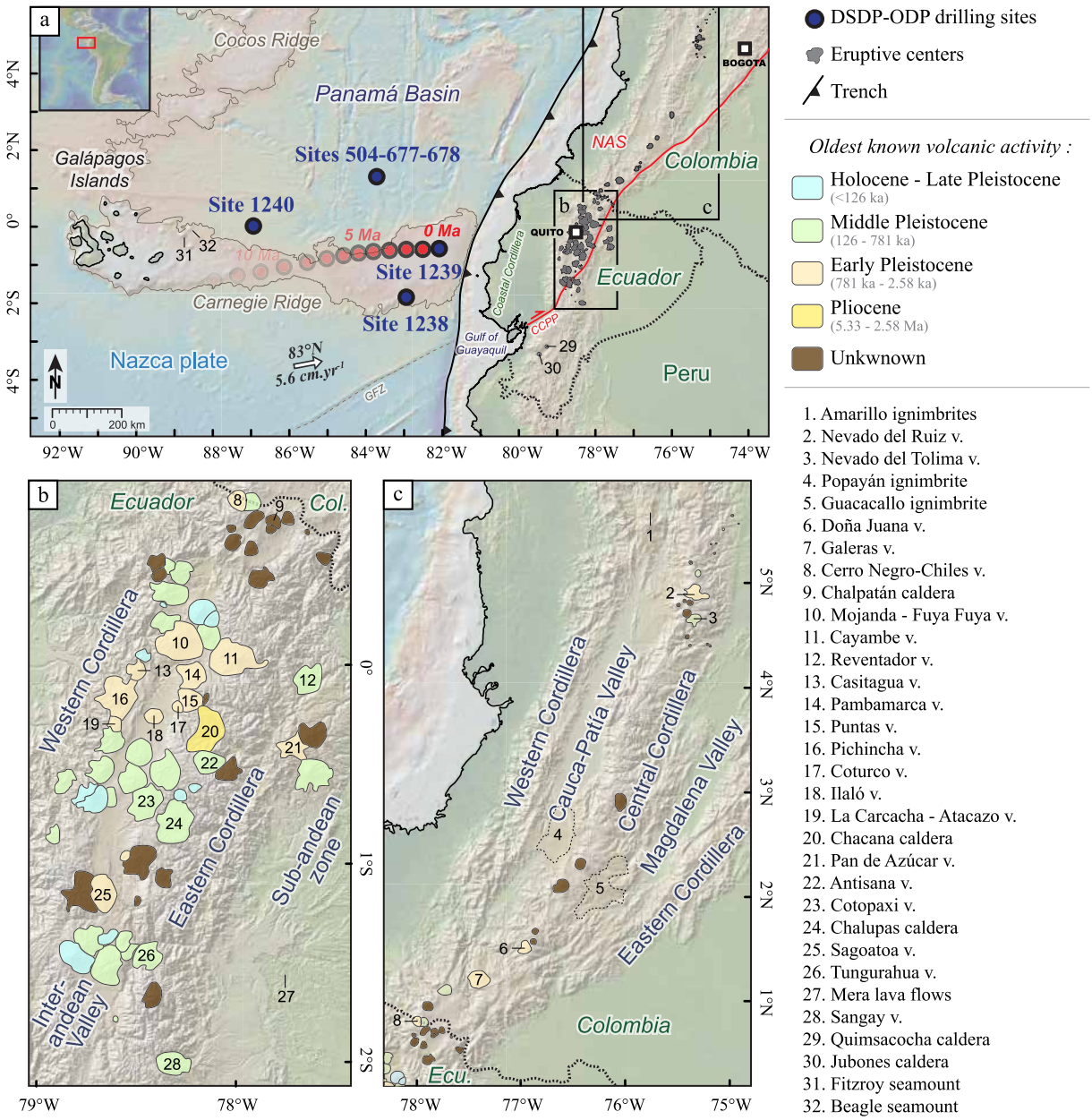

Figure 1. Geodynamic setting of the Northern Andes. (a) Map of Ecuador and the Galápagos Islands. Blue points represent the location of DSDP and ODP drilling sites presented in this work (Sites 1238, 1239 and 1240 from Leg 202 (Shipboard Scientific Party, 2003), Site 504 from Leg 69 (Shipboard Scientific Party, 1983), and Sites 677 and 678 from Leg 111 (Shipboard Scientific Party, 1988). Sites 678 and 504 are located 2.4 km NW and 4.4 km NNE of Site 677, respectively. Red points represent the tectonic backtrack path in million-year increments of ODP Site 1239, inferred from paleogeographic reconstructions of Daly (1989), Meschede and Barckhausen (2001), Sallarès and Charvis (2003) and Collot et al. (2009), and relative to a fixed South America. Ecuadorian and Colombian eruptive centers represented in brown. CCPP: Chingual-Cosanga-Pallatanga-Puná fault system, NAS: North Andean Sliver, GFZ: Grijalva Fracture Zone. (b–c) Maps of the Plio-Quaternary Ecuadorian and Colombian arcs, respectively. Colors refer to their oldest known activity, based on K-Ar on groundmass, $^{40}Ar/^{39}Ar$, fission track, or ^{14}C ages (Almeida et al., 2023; Andrade et al., 2021; Bablon, Quidelleur, Samaniego, et al., 2020; Bablon, Quidelleur, Siani, et al., 2020; Bablon et al., 2019; Béguelin et al., 2015; Bernard et al., 2014; Bigazzi et al., 1992; Hall & Mothes, 2008a, 2008b; Hall et al., 2017; Hidalgo, 2006; Hoffer, 2008; Monzier et al., 1999; Opdyke et al., 2006; Robin et al., 2009, 2010; Samaniego et al., 2005, 2012, 2022; Santamaría et al., 2022, 2023, 2024 for Ecuador, Bustos et al., 2023; Calvache et al., 1997; Monsalve et al., 2019; Moreno-Alfonso et al., 2021; Pardo et al., 2023; Thouret et al., 1990, 1995; for Colombia). v.: volcano.

plate coupling at the subduction interface). The timing of collision of the Carnegie Ridge, a basaltic plateau that corresponds to the track of the Galápagos hotspot activity on the Nazca plate (Figure 1a), is highly debated. Several authors propose that the Ridge subduction started between 0.5 and 3 Ma based on the development of volcanic activity, uplift of the Coastal Cordillera and forearc basins, or opening of the Gulf of Guayaquil (e.g.,

Cantalamessa & Di Celma, 2004; Graindorge et al., 2004; Lonsdale, 1978; Pedoja et al., 2006; Witt et al., 2006). Other studies support an age of 4–6 Ma, inferred from palaeogeographical reconstructions of the margin, spatial distribution of volcanoes, change in the geochemical signature of magmas, and exhumation ages (e.g., Barberi et al., 1988; Bourdon et al., 2002; Collot et al., 2009, 2019; Hall & Wood, 1985; Margirier et al., 2023). The oldest proposed ages range from 8 to 15 Ma, and are based on paleogeographic reconstructions and exhumation ages (Daly, 1989; Spikings et al., 2001, 2005). However, this wide time frame probably reflects the lack of clear correlation between tectonic deformations and Carnegie Ridge subduction (Gregory-Wodzicki, 2000; Michaud et al., 2009), and palaeogeographical reconstructions pointing to 4–6 Ma are likely more reliable. The fast (~6 cm/y; Nocquet et al., 2014) and oblique convergence (Figure 1a), combined with the subduction of the Carnegie Ridge, lead to the north-eastward displacement of the North Andean Sliver (NAS) along the Chingual-Cosanga-Pallatanga-Puná (CCPP) fault system, which extends from the Gulf of Guayaquil to the Caribbean Sea (Figure 1a; e.g., Alvarado et al., 2014). Furthermore, the oceanic crust is significantly younger north of the Grijalva Fracture Zone (GFZ, Figure 1a) than south of this escarpment (e.g., Hey, 1977; Lonsdale, 2005), which strongly controls the thermal regime of the slab-mantle system influencing in turn the geochemical slab component signature of magmas (Ancellin et al., 2017; Narváez et al., 2023). The complex structure of the subducting Nazca plate, with marked density, thickness and age contrast along the trench (see Part 1 in Bablon et al. (2025b)), is accountable for a slab flexure at about 1°S that accommodates the convexity of the margin (Yepes et al., 2016), and for a flat slab region south of 3°S, associated with a Quaternary volcanic gap (e.g., Gutscher et al., 2000).

2.2. The Volcanic Activity in the Northern Andes

From accretion of oceanic terranes in Ecuador and Colombia (Feininger & Bristow, 1980), and uplift of Andean cordilleras for example, (Spikings et al., 2001, 2005), the oldest remnants of a continental autochthonous volcanic arc in the Northern Andes are lavas and pyroclastic material, mainly of rhyolitic composition of Loma Blanca and Saraguro Formations (e.g., Hungerbühler et al., 2002; Vallejo et al., 2019). They crop out between 2 and 5°S, and were emitted between the Eocene and Early Miocene. They are coeval with the calc-alkaline andesitic lavas of the Oligo-Miocene San Juan de Lachas Formation, exposed near the Ecuador-Colombia boundary (e.g., Vallejo et al., 2019). West of Santa Isabel city, the Early Miocene Jubones Formation (#30, Figure 1a) is composed by four sequences of pyroclastic flow deposits and ignimbrites emplaced during Volcanic Explosivity Index (VEI) 6–7 eruptions (Armijos and Sánchez, 2018). Middle Miocene volcaniclastic sequences are recorded in the Zumbagua Formation in the Western Cordillera in Ecuador (e.g., Egüez et al., 2017; Vallejo et al., 2019), and north of 5°N in Colombia (e.g., Jaramillo et al., 2019). Andesitic to rhyolitic volcanic breccias, ash flows, pyroclastic flow deposits and ignimbrites emplaced during the Late Miocene volcanism comprise the Combia and the widespread Tarqui Formations, present in central Colombia and southern Ecuador, respectively (e.g., Bernet et al., 2020; Hungerbühler et al., 2002). The only described volcanic structure is the Quimsacocha caldera in southern Ecuador (#29, Figure 1a). It is surrounded by andesitic lavas and breccias emplaced during an early construction phase between ~9.5 and 7 Ma, and rhyolitic ignimbrites in distal areas that were associated with the formation of the caldera at about 5 Ma (Beate et al., 2001; Schütte et al., 2010a). Intracaldera dacitic and rhyolitic domes emplacement until ~3.5 Ma represents the final phase of the caldera's activity (Beate et al., 2001; Schütte et al., 2010a). Whereas the volcanic activity ceases south of 2°S and north of 5°N due to a flat configuration of the subducted slab (e.g., Gutscher et al., 1999; Wagner et al., 2017), volcanism continues during the Mio-Pliocene between 2°S and 3°N, resulting in pyroclastic deposits, andesitic lava flows, and volcaniclastic sediments of the Pisayambo Formation in the Eastern Cordillera of the northern half of Ecuador (Barberi et al., 1988; Egüez et al., 2017; Hall & Calle, 1982; Lavenu et al., 1992), and rhyolitic ignimbrites of the Popayán and Guacacallo Formations in southern Colombia (Alvarez Silva, 2022; Torres Hernández, 2010; Van der Wiel, 1991). The current arc, forming the Northern Volcanic Zone of the Andes (NVZ), is characterized by the construction of numerous andesitic stratovolcanoes and large silicic calderas (e.g., Barberi et al., 1988; Hall et al., 2008; Ramón et al., 2021). They are distributed in the Western and Eastern Cordilleras, Interandean Valley and Sub-Andean zone in Ecuador (Figure 1b), and along the Central Cordillera in Colombia (Figure 1c).

2.2.1. Geochronology of Products of the Current Arc

In Ecuador, the oldest volcanic deposits of the current arc sampled in the Cordillera are Late Pliocene in age. They correspond to the Mera lavas in the Sub-Andean zone (#27, Figure 1b), dated at 2.77 ± 0.07 Ma ($^{40}Ar/^{39}Ar$,

Hoffer et al., 2008), and to a lava located on the eastern flank of the Chacana caldera in contact with the underlying metamorphic rocks, that yields a poorly constrained $^{40}Ar/^{39}Ar$ age of 2.7 ± 0.2 Ma (#20, Figure 1b; Opdyke et al., 2006). The construction of stratovolcanoes started during the Early Pleistocene near 0° latitude, surrounding the current city of Quito (light orange volcanoes, Figure 1b). Based on $^{40}Ar/^{39}Ar$ and K-Ar on groundmass ages, oldest lavas belong to Pambamarca (#14, Figure 1b; 1.37 ± 0.02 Ma, Santamaría et al., 2024), Atacazo (#19; 1.29 ± 0.01 Ma, Hidalgo, 2006), Ilaló (#18; 1.27 ± 0.02 Ma, Santamaría, 2021), Puntas (#15; 1.13 ± 0.02 Ma, Santamaría et al., 2024), Guagua Pichincha (#16; 1.11 ± 0.02 Ma, Robin et al., 2010) and Cayambe (#11; 1.11 ± 0.01 Ma, Samaniego et al., 2005) volcanoes, and to the Pisque Formation sampled north of Quito (1.15 ± 0.03 Ma, Alvarado et al., 2014). The volcanic activity has intensified over the last 600 ka, and volcanism extended between 2°S and 1°N in both cordilleras (Bablon, Quidelleur, Samaniego, et al., 2020; Bablon et al., 2019; Santamaría et al., 2023, 2024; and references therein). This increase may have been caused by changes in deep (e.g., thermal regime in the slab and the mantle wedge, slab geometry, signature of slab components) and shallow/surface (e.g., tectonic activity, magma rise favored by basement-inherited fault systems and sutures) processes (Bablon et al., 2019; Santamaría et al., 2024). Radiocarbon age determinations show that at least 24 volcanoes were active during the Holocene, eight of them showing eruptive activity during Historical times (e.g., Hall et al., 1999, 2017; Hidalgo et al., 2008; Le Pennec et al., 2011, 2013; Samaniego et al., 1998), and two of them being currently in eruption (Reventador and Sangay, #12 and 28, Figure 1b). Transported westward by prevailing winds, ash emitted during Holocene eruptions of Guagua Pichincha, Atacazo-Ninahuilca and Cotopaxi volcanoes (VEI of 4–5) were found in marine sediments off Ecuador (Bablon et al., 2022). The largest Quaternary explosive event in the Northern Andes resulted in the formation of the Chalupas caldera at 216 ± 5 ka (VEI-7, #24, Figure 1b), and ash deposition as far as 900 km from source (Bablon, Quidelleur, Siani, et al., 2020).

Further north, volcanoes from the Colombian arc form a single row along the Central Cordillera, but their timing of construction is poorly constrained. The oldest dated lavas were emitted by the Doña Juana volcanic complex (#6, Figure 1c; 1.125 and 1.111 ± 0.004 Ma, Pardo et al., 2023). Some K-Ar ages yielded Early Pleistocene ages for basal lavas of Nevado del Ruiz volcano (#2; Thouret et al., 1990). These ages, though, should be considered with caution as they were carried out on whole-rock, and may include phenocrysts containing inherited radiogenic argon and/or weathered areas, possibly resulting in too old apparent ages. Most volcanoes of the current arc were active during the Late Pleistocene-Holocene and experienced explosive eruptions, including Azufral, Cerro Bravo, Cerro Machín, Doña Juana, El Escondido, Galeras and Nevado del Ruiz (e.g., Bustos et al., 2023; Calvache et al., 1997; Ceballos–Hernández et al., 2020; Monsalve et al., 2019; Murcia et al., 2008; Pardo et al., 2023; Williams et al., 2017).

2.2.2. Geochemistry of the Quaternary Arc

Volcanic products of the current arc mainly consist of lavas and tephra deposits with a mineral assemblage composed by plagioclase and pyroxene, and more rarely olivine, biotite, amphibole and quartz. Their composition is generally andesitic to dacitic, with extremely scarce basalts, basaltic andesites and rhyolites (e.g., Barberi et al., 1988; Droux & Delaloye, 1996; Hall et al., 2008). Magmas belong to the calc-alkaline magmatic series, showing a geochemical signature typical of continental arc magmas with enrichments in Large-Ion Lithophile Elements (LILE, such as Rb, Ba and K) and in Light Rare-Earth Elements (LREE, such as La, Ce and Nd) compared to Heavy Rare-Earth Elements (HREE, such as Dy, Er and Yb), and depletions in High Field Strength Elements (HFSE), notably Zr, Th, Nb and Ta, and a marked across-arc geochemical zonation (e.g., Ancellin et al., 2017; Droux & Delaloye, 1996; Hidalgo et al., 2012). In Ecuador, the arc is wider and volcanoes are distributed along different N-S alignments. Volcanic edifices located in the Eastern Cordillera and in the Sub-Andean zone release magmas that are more enriched in incompatible elements (K, Ba, Nb, Th, Y, Rb, Sr, Zr, and Rare Earth Elements, for instance) and have lower fluid-mobile to fluid-immobile elements ratios (Ba/Th, Ba/La, and Ba/Nb, for instance) than volcanoes from the volcanic front (Figure 2). This west-to-east geochemical zonation is interpreted to be related to a progressive decrease in the slab inputs coupled with a decrease of the degree of partial melting of the mantle wedge (e.g., Ancellin et al., 2017; Barragán et al., 1998; Hidalgo et al., 2012). Sr-Pb isotopic signature of Northern Andean magmas also exhibits an across-arc variation. Volcanoes located in the Eastern Cordillera in Ecuador and in Colombia exhibit higher $^{207}Pb/^{204}Pb$ ratios (>15.63, respectively; James & Murcia, 1984; Ancellin et al., 2017; Errázuriz-Henao et al., 2019) than those located in the Western Cordillera and in the Sub-andean zone. These latter also display lower $^{87}Sr/^{86}Sr$ ratios than volcanic center from the Eastern Cordillera and from Colombia (e.g., Ancellin et al., 2017; Errázuriz-Henao et al., 2019;

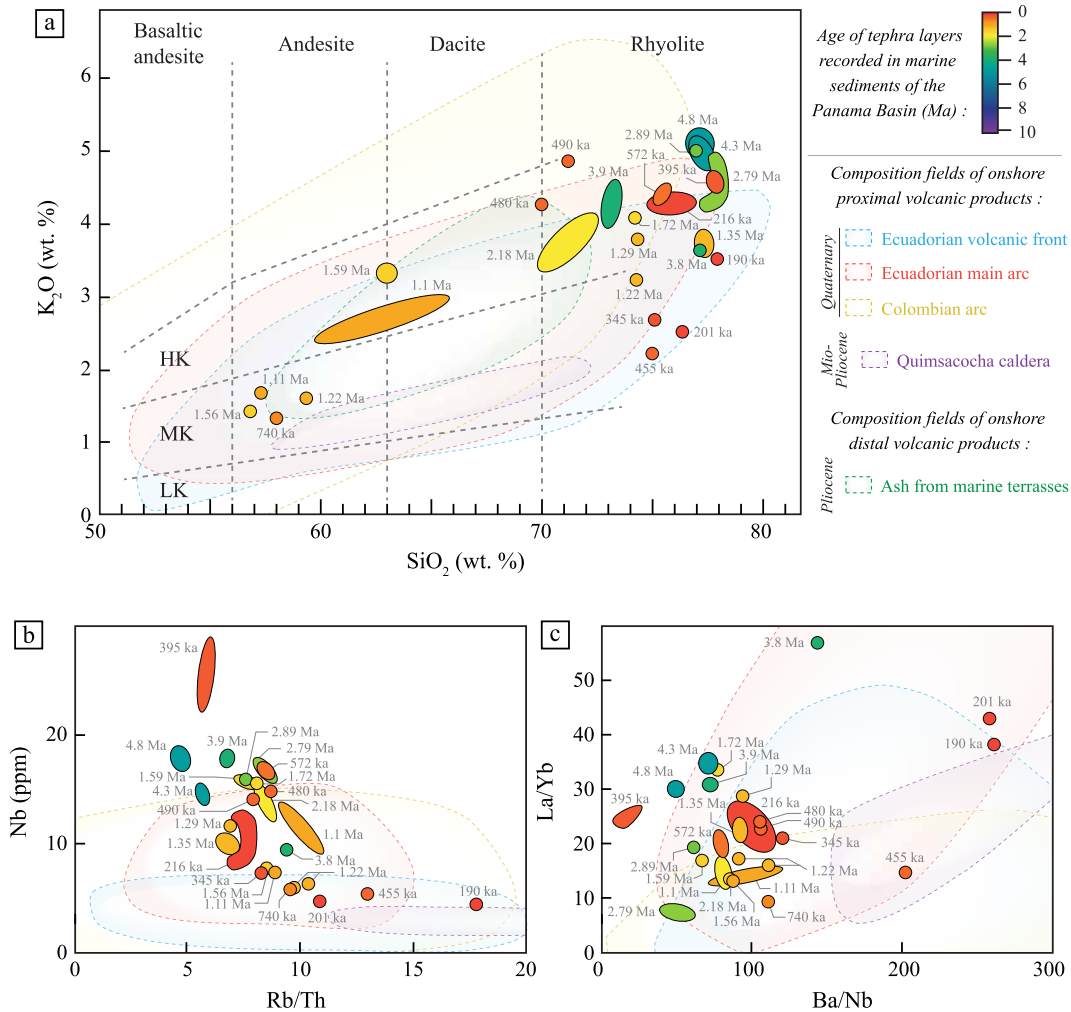

Figure 2. Comparison between the composition of tephra layers recorded in marine sediments in the southern part of the Panamá Basin, and the composition fields obtained for proximal volcanic material of the Ecuadorian and Colombian arcs (blue, red, and yellow fields; generally whole-rock measurements, Georoc database https://georoc.mpch-mainz.gwdg.de/georoc/), for products of the Mio-Pliocene Quimsacocha caldera (purple field; ICP-AES on whole-rock, Beate et al., 2001), and for ash layers recorded in Pliocene coastal sediments north of Ecuador (green field; XRF on whole-rock, Aalto & Miller, 1999). (a) K_2O versus SiO_2 diagram (Peccerillo & Taylor, 1976). HK: high-K, MK: medium-K, LK: low-K calc-alkaline magmatic series. Composition of marine tephra corresponds to average values measured on single glass shards, whereas measurements of onshore proximal products are generally performed on bulk rock of lavas, pumices, or juvenile blocks or pyroclastic flow deposits. Colors of symbols refer to the age of the tephra. (b) Nb (in ppm) versus Rb/Th. (c) La/Yb versus Ba/Nb (in ppm). The composition of our tephra samples measured on single grains is compared to that of on land products generally measured on whole-rock (i.e., including groundmass and crystals), which can explain that some analyses plot outside fields obtained for on land deposits. Uncertainty of ages are given in the text, Figure 3 and Table 1.

Hidalgo et al., 2012; James & Murcia, 1984; Laeger et al., 2013; Melson et al., 1990). Ancellin et al. (2017) interpret the isotopic variations of the Quaternary Ecuadorian volcanoes as reflecting an increase in the degree of crustal contamination in the southern part of the arc, as well as a decrease in the aqueous fluid/siliceous slab melt ratio away from 0.5°S, whereas Chiaradia et al. (2021) claim that magmas from the volcanic front edifices located in the inferred prolongation of the Carnegie Ridge are stored and evolve at greater depths to explain their lower Th, Nb, Nd and higher Ba/Th contents.

Despite a large number of eruptive centers active during the Quaternary in the Northern Andes, their mineralogy, major and trace elements contents, and Sr-Pb isotopic ratios display fairly large variations and diversity to allow us to determine the volcanic source of distal products, and in particular tephra preserved in continental and marine sedimentary sequences (Aalto & Miller, 1999; Bablon, Quidelleur, Siani, et al., 2020; Bablon et al., 2022, 2023;

Santamaría et al., 2017; Vallejo Vargas, 2011). In this work, we use major and trace elements concentrations and Sr-Pb isotopic data presented in the companion paper, in which procedures and standards used are detailed, and results of all analyses are available (Bablon et al., 2025b). Age models of tephra layers are based on bio- and magnetostratigraphy, $\delta^{18}O$ records and correlations between coring sites, and are also detailed in the companion paper (Bablon et al., 2025b, and referenced therein).

3. Results

3.1. Identification of the Volcanic Source of Northern Andean Distal Tephra Layers

The composition of tephra from the Northern Andes recorded in marine sediments off Ecuador is andesitic to rhyolitic, and belongs to the Medium- and High-K magmatic series (Figure 2a; Bablon et al., 2025b). The oldest products, of Pliocene age, have High-K rhyolitic compositions (blue-green symbols; Figure 2a), whereas Pleistocene samples have a wider range of composition (yellow-orange-red symbols; Figure 2a). Glass shards of six tephra layers emplaced between 1.59 Ma and 740 ka have an andesitic composition. The youngest tephra layers have rhyolitic glass compositions belonging to the Medium-K series.

Proximal products of the Quaternary arc sampled in the Cordillera generally belong to the Medium-K series for Ecuadorian frontal volcanoes, to the High-K series for volcanoes located in the Ecuadorian main arc (i.e., in the Interandean Valley and in the Eastern Cordillera), and present slightly higher K_2O content in Colombia (blue, red, and yellow domains, Figure 2a; e.g., Hidalgo et al., 2012; Ancellin et al., 2017 and references therein). Accordingly, the eruptive centers that emitted distal High-K tephra layers may be located in the main arc of Ecuador or in Colombia. Similarly, eruptive centers that emitted Medium-K tephra may be located in the volcanic front, which is consistent with low contents in Nb (Figure 2b). In addition, Colombian volcanoes display lower La/Yb values than most edifices from the Ecuadorian main arc (Figure 2c), which leads to the conclusion that distal ash layers with high La/Yb ratios were emitted by eruptive centers located in Ecuador.

Spider diagrams of incompatible elements of marine distal tephra normalized to the primitive mantle, grouped according to their similarity, are presented in Figure 3. Higher LILE enrichments together with negative anomalies in Sr are associated with tephra that belong to the High-K magmatic series (Figures 3a–3d), whereas tephra with lower LILE enrichments, in some cases accompanied by positive Sr anomalies, are those that belong to the Low-K magmatic series (Figures 3e and 3f). Strongest depletions in Sr are noted for tephra emplaced at about 2.89 Ma, 2.79 Ma and 395 ka (Figure 3c), and tephra emplaced at about 3.8 Ma, 201 ka and 190 ka exhibit the lowest HREE contents (Figure 3f). Colored domains represent ranges of values of eruptive centers that best match the composition of distal tephra, without considering their known activity period and eruptive style (comparison with each eruptive center is detailed in Data Set S1).

3.1.1. Pleistocene Tephra Layers

3.1.1.1. Dacitic and Rhyolitic Glass Composition Belonging to the High-K Magmatic Series

Few eruptive centers emitted products with a composition close to that of distal tephra belonging to the High-K series, except Chalupas and Chacana calderas, and Cotopaxi volcano (Figures 3a–3d), which belong to the Ecuadorian main arc (#24, 20 and 23, respectively, Figure 1b). The thickest tephra layer has already been correlated to the ***216 ± 5 ka*** Chalupas caldera deposits (VEI-7 eruption; Bablon, Quidelleur, Siani, et al., 2020), and the new isotopic data support this correlation (Figures 4 and 5). The three analyzed samples from two different coring sites (i.e., Sites 504 and 1239) display quite heterogeneous $^{207}Pb/^{204}Pb$ ratios, reflecting the isotopic variability of each volcano (Ancellin et al., 2017).

According to Córdova et al. (2020), the Chalupas caldera did not experience other large explosive events during its history, unlike the Chacana caldera that experienced major eruptions since 2710 ± 190 ka (Opdyke et al., 2006). A comparison of major and trace compositions of marine tephra with those of the proximal products sampled in Ecuador and Colombia reveal that tephra layers deposited at ***1.29 ± 0.01*** and ***1.72 ± 0.01 Ma*** on the one hand, and ***1.35 ± 0.01 Ma*** on the other, are similar to rhyolites from the Chacana caldera analyzed by MacDonald et al. (1992) and Bryant et al. (2006) (Data Set S2 graphs e, f), but whose age is unknown. No isotope measurements were performed for the ∼1.72 Ma tephra, but Sr and Pb isotopic ratios of the ∼1.29 Ma tephra support a source in the Chacana caldera (Figures 4 and 5). The Pb ratios of the 1.35 Ma tephra are closer to the isotopic trend of Nevado del Ruiz volcano (Figure 5b), but, as proximal products display significantly higher Sr

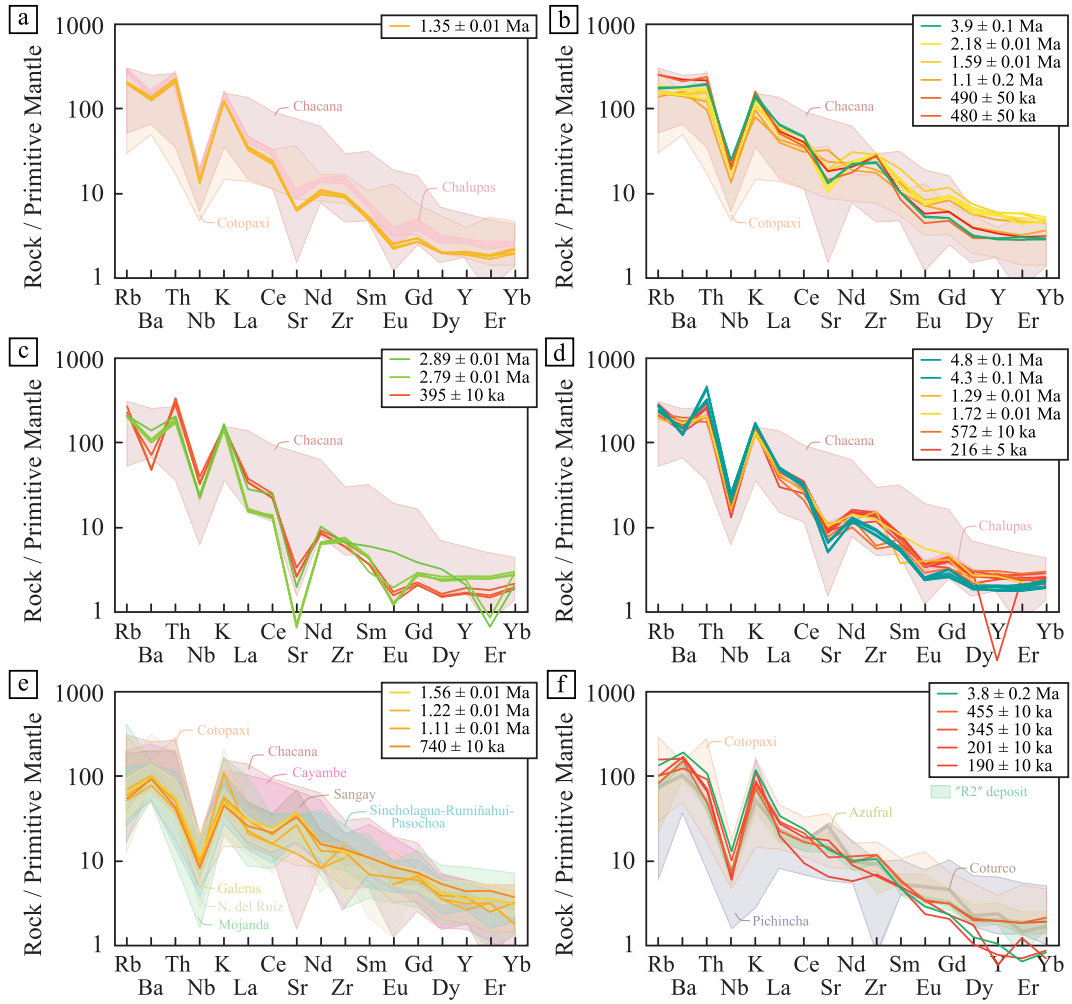

Figure 3. Incompatible elements normalized to primitive mantle spider diagram (Sun & McDonough, 1989) of tephra layers identified in the Panamá Basin, grouped based on their similarity. Color of spectra refers to the age model of the tephra (Figure 2). For the sake of clarity, colored domains represent the range of values obtained on onshore proximal deposits for eruptive centers that exhibit similar geochemical trends (Georoc database), but the whole data set is given in Data Set S1.

and lower Rb contents, we discard the hypothesis that this volcano could be the source of that tephra and infer that it was emitted by Chacana caldera.

The tephra with a High-K rhyolitic glass composition deposited at ***395 ± 10 ka*** is distinguished by low HREE contents, high Nb content (Figure 2b), marked depletions in Ba and Sr (Figure 3c), heterogeneous and rather low $^{206}Pb/^{204}Pb$ ratios (Figure 4a), and high $^{87}Sr/^{86}Sr$ ratios (Figure 4b). The Pb isotopy of the tephra is close to the signature (i.e., correlation line) of the Cayambe volcano (Figure 5b), but major-trace compositions strongly differ. Because our compositional data match none of those from previously studied volcanoes (Figure 5b), we assign them to an edifice from the Eastern Cordillera whose eruptive history is still poorly documented, for instance in the northernmost Ecuadorian arc.

The composition of the two tephra layers emplaced at ***480 and 490 ± 50 ka*** is quite close, with high K_2O and Nb contents (Figures 2a and 2b), which point to a source located in the Eastern Cordillera, and a slight enrichment in Sr (Figure 3b). No isotope measurements were performed for the ~490 ka tephra. Sr and Pb ratios of the ~480 ka tephra are close to the range of values of Cayambe and Cotopaxi volcanoes, and Chacana caldera (Figure 5). Cayambe volcano was not active, or experienced no major explosive events at about 450–500 ka (Samaniego et al., 2005), this source can therefore be discarded. Opdyke et al. (2006) provided poorly constrained $^{40}Ar/^{39}Ar$ ages of 440 ± 150 and 450 ± 80 ka from lavas assigned to the activity of Chacana, revealing that the caldera was

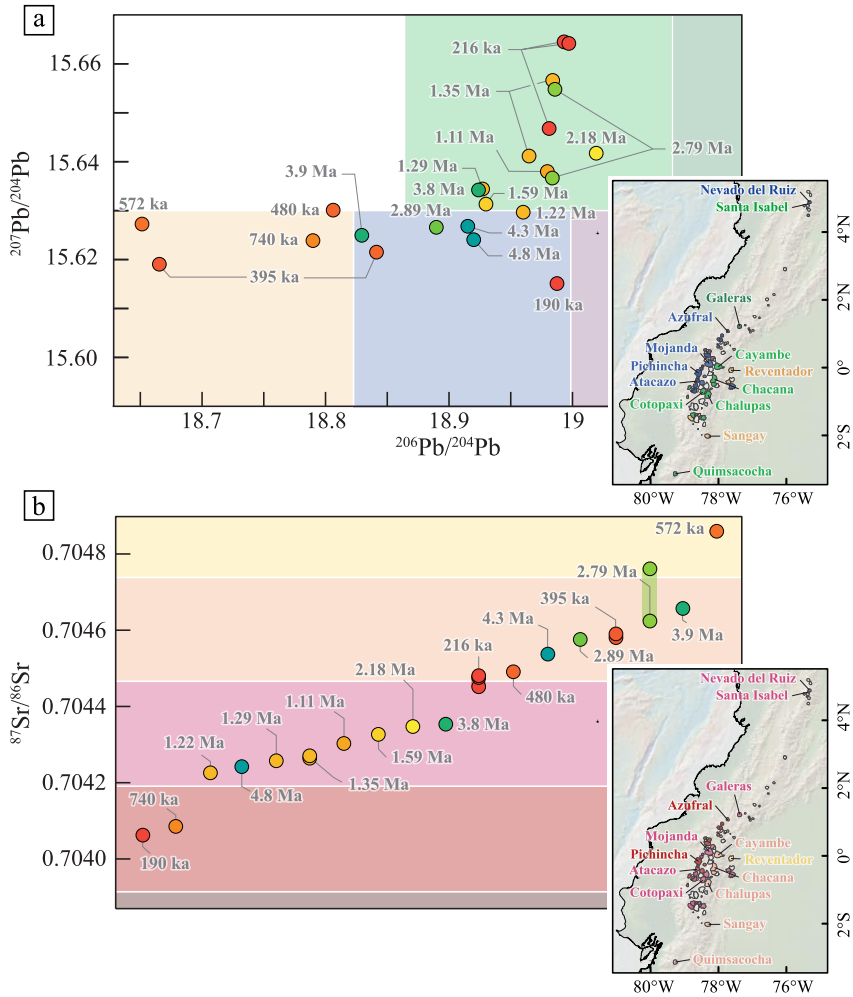

Figure 4. Comparison between the composition of tephra from the Panamá Basin and the lead and strontium isotopic composition fields obtained in Ecuador and Colombia (James & Murcia, 1984; Melson et al., 1990; Schütte, 2009; Laeger et al., 2013; Ancellin et al., 2017 and references therein; Errázuriz-Henao et al., 2019; Chiaradia et al., 2020). (a) $^{207}Pb/^{204}Pb$ versus $^{206}Pb/^{204}Pb$ diagram. (b) $^{87}Sr/^{86}Sr$ results obtained for marine tephra layers presented from the smallest to the largest ratio. The maps on the right indicates the average of published ratios obtained on proximal products. The isotopic signature of magmas located away from the trench is more influenced by the isotopic signatures of the mantle wedge and continental crust, whereas the slab isotopic signature is stronger for volcanoes located in the frontal arc, where the mantle wedge is thinner (Ancellin et al., 2017; Hidalgo et al., 2012). Same symbols of offshore tephra as Figure 2. Uncertainty of ages are given in the text, Figure 3 and Table 1.

active during that period. However, no geochemical data are available for these proximal samples, and no pyroclastic deposits associated with the caldera have been described so far in the Cordillera at about 450–500 ka. The oldest deposits relative to Cotopaxi volcano define the Barrancas rhyolite series, made up of thick deposits of ash flows, block-and-ash flows, and tephra falls, emplaced between ~560 and 420 ka (Hall & Mothes, 2008a). Few geochemical data are available, and the ~480 and 490 ka tephra layers have higher LILE and HFSE contents than the oldest proximal obsidian flow dated at 537 ± 11 ka (K-Ar on volcanic glass, Santamaría et al., 2023, Data Set S2 graph d). However, considering the high explosivity of Cotopaxi during that period, it is the most likely source of the two distal tephra layers.

The tephra layer emplaced at ***572 ± 10 ka*** has a composition in major and trace elements close to that of products from the Eastern Cordillera of Ecuador, and from the Central Cordillera of Colombia (Figure 2). However, it displays the highest $^{87}Sr/^{86}Sr$ and the lowest $^{206}Pb/^{204}Pb$ ratios among our tephra collection (Figure 4). Such ratios were not reported for Ecuadorian products so far. However, we exclude that the volcanic source of this tephra is located in Central America or in the current Peruvian arc, because magmas display significantly lower

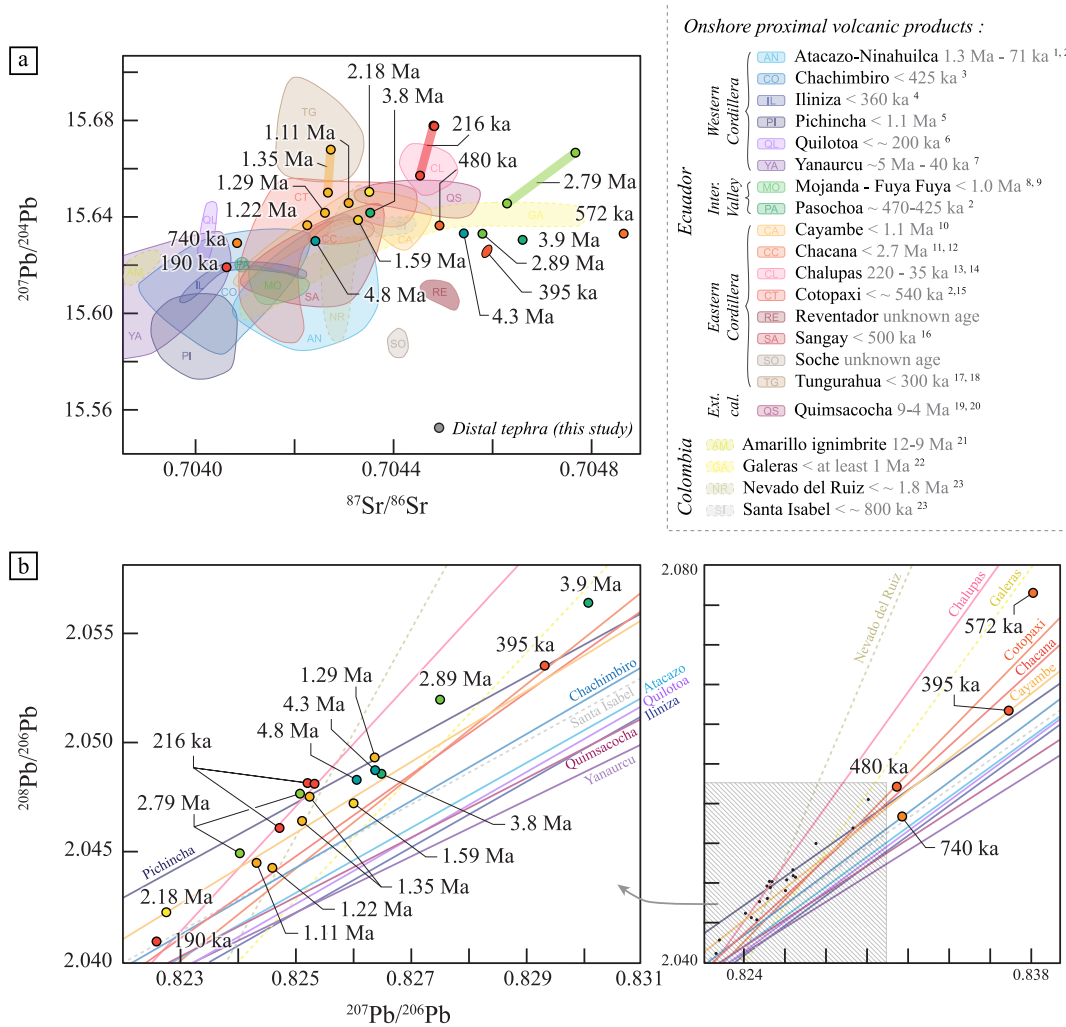

Figure 5. Comparison between strontium and lead ratios of distal tephra and those of onshore proximal products (this work and Georoc database, respectively). We have included volcanoes for which no explosive activity has been documented, so as not to rule out the possibility that they may have been explosive during their history, and may be the source of distal tephra. (a) $^{207}Pb/^{204}Pb$ versus $^{87}Sr/^{86}Sr$ diagram. The global period of activity of eruptive centers is indicated in gray in the caption, from ages published in [1] Hidalgo (2006), [2] Santamaría et al. (2023), [3] Bellver-Baca et al. (2020), [4] Santamaría et al. (2022), [5] Robin et al. (2010), [6] Hall and Mothes (2008b), [7] Béguelin et al. (2015), [8] Bablon, Quidelleur, Samaniego, et al. (2020), [9] Robin et al. (2009), [10] Samaniego et al. (2005), [11] Opdyke et al. (2006), [12] Hall and Mothes (2008c), [13] Bablon, Quidelleur, Siani, et al. (2020), [14] Córdova et al. (2020), [15] Hall and Mothes (2008a), [16] Hall et al. (1999), [17] Hall et al. (1999), [18] Bablon et al. (2018), [19] Beate et al. (2001), [20] Schütte et al. (2010b), [21] Bernet et al. (2020), [22] Calvache et al. (1997), [23] Thouret et al. (1990). (b) $^{208}Pb/^{206}Pb$ versus $^{207}Pb/^{206}Pb$ diagram. These isotopic lines are independent of the age and type of material analyzed (i.e., glass shards, groundmass or minerals, from basaltic to rhyolitic magmas), and constitute a distinctive "fingerprint" of volcanic sources (Bablon et al., 2023). The analytical dispersion together with the large number of edifices in the Northern Andes and their relatively close magma genesis processes prevent to accurately define the volcanic vent associated with our distal tephra, but allow to point to three or four potential sources. For clarity, eruptive centers whose activity started during the past 190 kyr (i.e., Corazón, Cuicocha, Imbabura, Parulo, Pilavo, Puñalica, Pululahua, in activity after the deposition of the youngest tephra), or whose $^{87}Sr/^{86}Sr$ ratio is lower than 0.7039 or higher than 0.7048 (i.e., Pulumbura, Cerro Machín), have not been represented. Inter.: Interandean, Ext. cal.: extinct caldera. Uncertainty of ages are given in the text, Figure 3 and Table 1.

$^{207}Pb/^{206}Pb$ and higher $^{87}Sr/^{86}Sr$ ratios, respectively (Bablon et al., 2025b). We therefore infer that its source is located in the NVZ, and more likely in Colombia where isotopic data are scarce. Sr and Pb isotopic ratios of the tephra are close to products from Galeras volcano in Colombia (Figure 5). Although no analyzed proximal product of this eruptive center has a rhyolitic composition, Galeras volcano experienced a major explosive eruption at 560 ± 40 ka, resulting in the formation of a 5-km diameter summit caldera (end of Coba Negra stage,

Calvache et al., 1997). Accordingly, this event could be correlated to the 572 ± 10 ka tephra identified in marine sediments, which also allows us to improve the accuracy of the age of the formation of the summit caldera.

Major and trace element contents of tephra emplaced at ***1.1 ± 0.2***, ***1.59 ± 0.01*** and ***2.18 ± 0.01 Ma*** point to a volcanic source located in the Eastern Cordillera of Ecuador or Central Cordillera in Colombia (Figure 2). The proximal products with the closest composition are those erupted from the Chacana caldera (Figure 3b), but they have lower Zr and slightly higher Th/Yb ratio. The Popayán and Guacacallo Formations (#4 and 5, Figure 1c) are composed of thick high-K rhyolitic ignimbrites dated from ∼2.1 to 3.3 Ma (Alvarez Silva, 2022; Torres Hernández, 2010; Van der Wiel, 1991). As proximal deposits have significantly higher Sr contents and lower Sm, Nd, Zr and HREE contents than the ∼2.18 Ma tephra, as well as the 2.79 and 2.89 Ma tephra mentioned before (Data Set S2 graph g), they do not correlate. As the Sr and Pb isotopic ratios of tephra layers are consistent with the range of values obtained for the Chacana caldera (Figures 4 and 5) it is the most likely source of the ∼1.1, 1.59 and 2.18 distal tephra.

3.1.1.2. Andesitic Glass Composition Belonging to the Medium-K Magmatic Series

Tephra samples with andesitic glass shards belong to the Medium-K series (Figure 2a), and have the lowest contents in incompatible elements related to their lower differentiation degree (e.g., Figure 3e). As the distinction between products from volcanoes located in the volcanic front and in the main arc is more challenging for low silica contents (Figure 2a), we performed hierarchical cluster analysis (HCA) to statistically compare the composition of distal tephra and published onland products of Colombian and Ecuadorian edifices. We used major and trace element average contents, considering only proximal products with SiO_2 contents ranging from 55 to 62 wt.%. We then performed a second HCA with each distal tephra and the whole data set of closest edifices, to identify onland products with the closest composition. Graphs showing the comparison between these products and distal tephra, using the most discriminating chemical elements, are available in Data Set S2.

The closest proximal products of the ***740 ± 10 ka*** tephra are from the Galeras and Tungurahua volcanoes, and especially samples of three lava blocks of the oldest sector collapse of Tungurahua (Bablon et al., 2018, Data Set S2 graph h). However, the oldest dated lava of Tungurahua, in contact with the metamorphic basement, is significantly younger at ∼300 ka, although the avalanche may have incorporated and transported older material. In addition, the tephra presents a lower $^{207}Pb/^{204}Pb$ ratio than products from Tungurahua (Figure 5a). Isotopes are closer to products from Chachimbiro and Santa Isabel volcanoes (Figure 5b), but these edifices exhibit lower contents in most incompatible elements (Data Set S2 graph h). An obsidian lava plateau was emplaced north of the Chacana caldera between 0.75 and 0.98 Ma (whole-rock K-Ar ages from Barberi et al., 1988; and fission tracks from Bigazzi et al., 1992). However, the ∼740 ka tephra is unlikely related to this event, as glass shards exhibit significantly lower Rb, Th, and higher HREE contents. Consequently, no known proximal deposit clearly correlates with this tephra layer.

The ***1.11 ± 0.01 Ma*** tephra has major-trace element contents close to proximal products of Huisla, Igualata, Cotopaxi and Chimborazo volcanoes (Data Set S2 graph i), but the construction of these edifices started much later, during the Middle Pleistocene (Bablon et al., 2019; Samaniego et al., 2012). Sr-Pb isotopic ratios are closer to products from Cayambe volcano (Figure 5), and contents in incompatible elements of glass shards are compatible with this edifice (Figure 3e). The age model of the tephra corresponds to the early stage of construction of Viejo Cayambe, which may be the source of the tephra. However, this correlation should be considered with caution, as Viejo Cayambe experienced mainly effusive eruptions during this period (Samaniego et al., 2005).

The ***1.22 ± 0.01 Ma*** tephra has major-trace element contents close to proximal products of Sincholagua, Carihuairazo volcanoes, and Quimsacocha caldera (Data Set S2 graph j). Sr-Pb isotopic ratios of the tephra and products of the Quimsacocha caldera differ significantly (Figure 5b). Spectra of incompatible elements of Sincholagua, Rumiñahui and Pasochoa volcanoes, located south of Quito and emplaced between ∼500 and 200 ka (Santamaría et al., 2023), strongly agree with the ∼1.22 Ma tephra (Figure 3e). No Pb isotopic data are available for these edifices. $^{87}Sr/^{86}Sr$ ratios of Sincholagua, though, range from 0.7041 to 0.7045 (Francis et al., 1977; Harmon et al., 1984), matching with that of the tephra (Figure 5a). Similarly, the only isotopic measurement obtained on a product from Carihuairazo roughly compares to that of the tephra (0.7041 and 15.635 for $^{87}Sr/^{86}Sr$ and $^{207}Pb/^{204}Pb$ ratios; Ancellin et al., 2017), but the early stage of activity of the volcano occurred at about 0.5 Ma (Bablon et al., 2019). Accordingly, we infer that the ash was emitted during the activity of an old

stratovolcano, located in the central or southern part of the Ecuadorian arc, and whose products were subsequently concealed by younger lavas and deposits, or largely dismantled by erosion.

The major-trace elements composition of the ***1.56 ± 0.01 Ma*** tephra that has the lowest SiO_2 content in our tephra collection (Figure 2a) does not seem to correspond to any sample analyzed in the Northern Andean Cordillera. Unfortunately, we were unable to perform isotopic analysis because of the small amount of glass shards, and the source of the tephra remains unknown.

3.1.1.3. Rhyolitic Glass Composition Belonging to the Medium-K Magmatic Series

Among Pleistocene samples with medium-K rhyolitic compositions, tephra layers deposited at 201 ± 10 and 190 ± 10 ka have markedly low HREE contents (Figure 3f) that does not clearly match with any known magmatic composition in our data set. In particular, the major and trace element composition of the ***190 ± 10 ka*** tephra significantly differs from that of the regionally dispersed "Pifo" tephra layer (SiO_2 = 76.6 wt.%, K_2O = 4.5 wt.%; Bablon, 2018), deposited north of Ecuador between 220 ± 20 and 150 ± 20 ka (Bigazzi et al., 1992; Hall & Mothes, 1997). The ∼190 ka tephra is also depleted in most incompatible elements compared to Mullumica, Callejones and Potrerillos obsidian flows, which correspond to the most recent rhyolitic emissions of the Chacana caldera (Bigazzi et al., 1992; Hall & Mothes, 2008c). Major and trace element contents of the ∼190 ka tephra layer support a source in the Ecuadorian volcanic front (Figure 2), supported by low $^{207}Pb/^{204}Pb$ and $^{87}Sr/^{86}Sr$ ratios (Figure 4), and which may be Chachimbiro volcano based on Pb isotopic lines (Figure 5b). However, few ages are available to constrain the eruptive history of this edifice, and they suggest that it was not active from ∼265 to 145 ka (Bellver-Baca et al., 2020). We were unable to measure Sr and Pb ratios of the ***201 ± 10 ka*** tephra layer, but its major-trace composition points to a source located in the Western Cordillera (Figure 2) and is close to that of sample "ALS 61" from Almas Santas volcano (Hidalgo et al., 2012, Data Set S2 graph c). Only two K-Ar ages of lavas are available for this edifice, but they are older than the distal tephra (374 and 364 ± 7 ka, Santamaría et al., 2023). Additional geochemical and geochronological data are therefore required to check the correlation to the ∼190 and ∼201 ka tephra layers.

Finally, the tephra emplaced at ***455 ± 10 ka*** has a composition very close to that of the voluminous "R2" deposit of rhyolitic pumices (Figure 3f, Data Set S2 graph b), emitted during a Plinian eruption of Fuya Fuya volcano that occurred at 476 ± 38 ka (Bablon, Quidelleur, Siani, et al., 2020; Robin et al., 2009). Although isotopic data would be useful to confirm their correlation, we infer that these deposits belong to a single volcanic event. Despite slightly higher K_2O and Th, and lower Ba contents, the composition of the ***345 ± 10 ka*** tephra is close to that of the ∼455 ka tephra (Figures 2a and 3f). On the southern flank of Fuya Fuya volcano, block-and-ash flow deposits related to dome activity interlayered with pumice lapilli and ash fall deposits were emplaced during eruptive cycles that lasted until about 340 ka (Bablon, Quidelleur, Siani, et al., 2020; Robin et al., 2009). On the other hand, the composition of the ∼345 ka tephra is also very close to that of proximal rhyolitic samples from Cotopaxi volcano (Data Set S2 graph a). However, no explosive eruptions are dated there from ∼420 to 20 ka (Hall & Mothes, 2008a), and major elements rather point to a source located in the volcanic front (Figure 2). Unfortunately, we were not able to measure the Sr and Pb ratios of the tephra due to the too small amount of glass shards, which would allow us to investigate whether Fuya Fuya volcano is indeed the source of the ∼345 ka tephra.

3.1.2. Pliocene Tephra Layers

The major and trace element contents of the tephra layer emplaced at ***2.79 ± 0.01 Ma*** are typical of products emitted by volcanoes from the Eastern Cordillera of Ecuador and from the Central Cordillera of Colombia (Figures 2 and 3), but its Sr and Pb isotopic ratios rather point to the Eastern Cordillera (Figure 4). Similarly, the ***2.79 ± 0.01 Ma***, ***3.9 ± 0.1 Ma***, and ***4.3 ± 0.1 Ma*** tephra layers have compositions characteristic of products from the Eastern Cordillera, with high K_2O and incompatible element contents (Figures 2 and 3), and $^{87}Sr/^{86}Sr$ ratios of about 0.7046 (Figure 4b). Their Sr and Pb isotopic ratios are close to products from Galeras volcano in Colombia (Figure 5). The oldest construction stages of Galeras are poorly constrained in time, but its activity may have started at ∼1.1 Ma (Calvache et al., 1997). This age corresponds to one of the largest lifespans of Quaternary volcanoes in the Northern Andes, and it is unlikely that any ash older than 2.7 Ma was sourced at this edifice. Therefore, they may have been emitted by an old eruptive center located in the Eastern Cordillera of Ecuador, with an isotopic signature close to that of Galeras volcano. Proximal products of this eruptive center could be part of the Pisayambo Formation, which crops out along the Eastern Cordillera (Egüez et al., 2017).

The tephra emitted at ***3.8 ± 0.2 Ma*** differs from the other Pliocene tephra, with medium-K rhyolitic glass compositions, significantly lower HREE contents (Figures 2c and 3f), and lower $^{206}Pb/^{204}Pb$ and $^{87}Sr/^{86}Sr$ ratios (Figure 4). It is also different from the Colombian ignimbrites belonging to the Popayán and Guacacallo Formations, which have lower K_2O and incompatible elements contents, especially HREE (Data Set S2 graph g). Accordingly, we infer that no proximal deposits assigned to this eruption have been analyzed yet, and that the ∼3.8 Ma ash has been likely emitted by a presently eroded, covered by Pleistocene products, or not yet studied, eruptive center, likely located in the Eastern Cordillera of Ecuador (Figure 2).

Finally, the tephra layer emplaced at ***∼4.8 Ma*** has a significantly lower $^{87}Sr/^{86}Sr$ ratio (Figures 4b and 5a), closer to products of the Chacana caldera. This source seems unlikely because such a long period of activity is not documented in the Northern Andes, but it should not be totally discarded as such durations were reported for rhyolitic eruptive centers from the Central Andes. As major and trace elements are typical of the main arc of Ecuador (Figure 2), the source of the tephra was likely located in the Eastern Cordillera. As for previous samples, proximal products of this old eruptive center could be part of the Pisayambo Formation, which remains poorly known so far.

3.1.3. Summary

Few major eruptions identified in marine sediments can be reliably correlated to proximal products (Table 1). Our work therefore highlights that despite the detailed geochemical and geochronological study of many Ecuadorian edifices conducted over several decades, the catalog of past major eruptions is incomplete. This demonstrates the importance of continuing investigation and accurate description of volcanic units on land, and to complement them with the study of tephra preserved in marine or lake sediments, especially in regions where many volcanoes have been active over a limited area, as in the Northern Andes. In addition, some key structures and formations, such as the Chalpatán caldera or Pisayambo/Tarqui deposits, have been little studied so far. For instance, no geochemical analyses have been published for the Chalpatán caldera, located in the Interandean Valley at the Ecuador-Colombia frontier (#9, Figure 1b). Only two poorly constrained whole-rock K-Ar ages of ∼1.2 and 2.1 Ma are available (Barberi et al., 1988), but the precise sampling sites are not provided, and the reliability of whole-rock K-Ar ages can be questioned (e.g., Bablon, Quidelleur, Samaniego, et al., 2020; Bablon et al., 2018). Field work, and geochemical and geochronological analyses would be therefore useful to investigate its eruptive history, and to identify if the caldera results from a single or multiple explosive events, and whether it could be the volcanic source of the distal tephra layers.

3.2. Characterization of Tephra With a CVZ-Like Signature

Two high-K rhyolitic tephra layers have a geochemical signature, in particular very high $^{87}Sr/^{86}Sr$ ratios (∼0.707), similar to Quaternary products from volcanoes of the Central Volcanic Zone (CVZ) of the Andes. These tephra layers have been identified at Sites 1238 and 1239, the closest to the margin (Figure 1), and have been deposited at 4.7 ± 0.3 and 8.9 ± 0.5 Ma, respectively. In southern Peru, thick ignimbrites result from four phases of intense volcanism that occurred between the Early Miocene and the Middle Pleistocene, in response to the uplift of the Andes and thickening of the crust (e.g., Paquereau-Lebti et al., 2006; Thouret et al., 2016; Vatin-Perignon et al., 1996). Ignimbrites emplaced during the Late Miocene at about 9 Ma (i.e., the Caraveli sheet that extensively covers high plateau of southern Peru, e.g., Thouret et al., 2007, 2016; Mamani et al., 2008; orange field, Figures 6a and 6b) and during the Pliocene (i.e., the composite, multi-layered sheet of the Lower Sencca Group; Thouret et al., 2016; Mamani et al., 2008; yellow field, Figures 6a and 6b) exhibit significantly lower HREE contents than our tephra samples, reflecting a deep magma genesis in a region characterized by a thickened continental crust (e.g., Davidson et al., 1990). In marine sediments off central Peru, Pouclet et al. (1990) identified several tephra layers. They suggested that ash layers of Eocene to Miocene age resulted from eruptions in a currently inactive arc in central and northern Peru, and attributed those of Pliocene and Pleistocene ages to the southern Peruvian arc (dark and light blue fields, Figure 6a). The tephra layer deposited at ***8.9 ± 0.5 Ma*** at Site 1239, has major element contents close to that of their ∼12.0 and 9.9 Ma tephra samples, but they did not perform trace element measurements, which would be needed to check this correlation. In northern Peru, volcanic products emitted by calc-alkaline andesitic volcanoes and calderas were emplaced from the Eocene to the Middle Miocene, and from the Late Miocene to the Early Pliocene (i.e., Calipuy Group and Yungay ignimbrites, respectively, dark and light green fields in Figures 6a and 6b; e.g., Hollister & Sirvas, 1978; Petford & Atherton, 1994; Rivera et al., 2005). Unlike products of the CVZ, magmas of the Calipuy Group are enriched in HREE,

Geochemistry, Geophysics, Geosystems

10.1029/2025GC012278

Table 1
Summary of Features of Marine Tephra Layers With a Geochemistry Typical of the Northern Andean Arc Identified in the Southern Part of the Panamá Basin

Epoch	Samples	Top depth of the tephra layer (in mcd)	Age	Thickness of tephra layers (cm)	Estimated VEI	Location of the vent based on geochemistry			Eruptive center that best matches age and geochemistry	Reliability of the correlation and comments
						Major and trace elements	Sr-Pb isotopes	Summary		
Middle Pleistocene	1239A-2H2-13	5.16	**190 ± 10 ka**	3	**5–6**	WC	WC, or CC	**WC**	Chachimbiro (Ecuador)	Weak (no large eruption identified on land for Chachimbiro volcano, and the volcano was not active during this period)
	1239C-1H4-68	5.57	**201 ± 10 ka**	2	**5–6**	WC	–	**WC**	Almas Santas (Ecuador)	Weak (few ages are available for this volcano and are older, and we were unable to measure Sr and Pb ratios of the distal tephra)
	504-1H2-77	12.20	**216 ± 5 ka**	1–40	**7**	EC	EC	**EC**	Chalupas caldera (Ecuador)	Very strong
	504-2H1-59									
	677A-2H2-80	9.00								
	677A-2H2-142									
	1238A-2H6-4	13.10								
	1239A-2H3-44	6.65								
	1239C-1H4-87									
	1239A-2H3-24									
	1240B-3H5-13	25.70								
	1240C-3H2-134									
	1239A-2H6-38	11.42	**345 ± 10 ka**	<1	**5–6**	WC, or CC	–	**WC, or CC**	Fuya Fuya (Ecuador)	Pretty weak (no isotopes measurements for the distal tephra)
	677B-2H6-73	15.72	**395 ± 10 ka**	3–8	**6**	EC	EC	**EC**	No volcanoes identified	–
	1239B-2H4-93	13.25								
	1240A-5H2-98	39.76								
	1238B-3H6-10	27.63	**455 ± 10 ka**	3	**5–6**	WC, or CC	–	**WC, or CC**	Fuya Fuya (Ecuador)	Medium (no isotopes measurements for the distal tephra)
	1238C-4H3-46	28.23	**480 ± 50 ka**	5	**5–6**	EC	EC	**EC**	Cotopaxi (Ecuador)	Medium (few data are available for the proximal deposits of

Geochemistry, Geophysics, Geosystems

10.1029/2025GC012278

Table 1
Continued

Epoch	Samples	Top depth of the tephra layer (in mcd)	Age	Thickness of tephra layers (cm)	Estimated VEI	Location of the vent based on geochemistry			Eruptive center that best matches age and geochemistry	Reliability of the correlation and comments
						Major and trace elements	Sr-Pb isotopes	Summary		
										the Barrancas rhyolitic series, emplaced between ~560 and 420 ka)
	1238B-3H6-96	28.50	**490 ± 50 ka**	4	**5–6**	EC	–	**EC**	Cotopaxi (Ecuador)	Medium (few data are available for the proximal deposits of the Barrancas rhyolitic series, emplaced between ~560 and 420 ka)
	1238B-4H3-97 1239A-3H4-74	34.27 19.54	**572 ± 10 ka**	4–6	**5–6**	EC, or CC	Typical of any region in Ecuador	**CC**	Galeras (Colombia)	Quite good (age and geochemistry match the explosive eruption resulting in the formation of a large summit caldera, but no rhyolitic products associated with this event have been described on land)
	504-5H1-112	28.70	**740 ± 10 ka**	1	**5–6**	WC, EC, or CC	WC, EC, or CC	**WC, EC, or CC**	No volcanoes identified	–
Early Pleistocene	1238B-6H5-79 1238C-7H1-108	60.28	**1.1 ± 0.2 Ma**	2–3 (diffuse)	**5–6**	EC, or CC	–	**EC, or CC**	Chacana caldera (Ecuador)	Medium (the tephra composition matches that of Chacana caldera's products, but we are unable to correlate it with a specific proximal deposit)
	1239B-6H3-36	52.73	**1.11 ± 0.01 Ma**	12 (diffuse)	**5–6**	WC, EC, or CC	WC, EC, or CC	**WC, EC, or CC**	Viejo Cayambe volcano (Ecuador)	Weak (Cayambe experienced mainly effusive volcanism during this period)
	1239A-7H3-130	60.39	**1.22 ± 0.01 Ma**	5 (diffuse)	**5–6**	WC, EC, or CC	WC, EC, or CC	**WC, EC, or CC**	No volcanoes identified	Petrogenetic processes similar than that those of products from

Geochemistry, Geophysics, Geosystems

10.1029/2025GC012278

Table 1
Continued

Epoch	Samples	Top depth of the tephra layer (in mcd)	Age	Thickness of tephra layers (cm)	Estimated VEI	Location of the vent based on geochemistry			Eruptive center that best matches age and geochemistry	Reliability of the correlation and comments
						Major and trace elements	Sr-Pb isotopes	Summary		
										Sincholagua, Rumiñahui, Pasochoa and Carihuairazo volcanoes
	1239B-7H3-123	63.48	**1.29 ± 0.01 Ma**	3	**5–6**	EC	WC, EC, or CC	**EC**	Chacana caldera (Ecuador)	Good
	1238A-8H2-14 1238B-7H5-140 1239B-7H6-66 1239C-8H5-72	71.58 67.43 	**1.35 ± 0.01 Ma**	4–14	**6**	EC	WC, EC, or CC	**EC**	Chacana caldera (Ecuador)	Pretty weak (Sr and Pb isotopes do not completely match those of Chacana caldera)
	1239C-8H5-37	80.35	**1.56 ± 0.01 Ma**	2	**5–6**	WC, EC, or CC	-	**WC, EC, or CC**	No volcanoes identified	–
	1238A-9H2-83 1239A-9H5-123	80.19 84.46	**1.59 ± 0.01 Ma**	2–3, diffuse until 6	**5–6**	EC, or CC	WC, EC, or CC	**EC, or CC**	Chacana caldera (Ecuador)	Medium (the tephra composition matches that of Chacana caldera's products, but we are unable to correlate it with a specific proximal deposit)
	1239A-12H2-94	91.14	**1.72 ± 0.01 Ma**	3 (diffuse)	**5–6**	EC	–	**EC**	Chacana caldera (Ecuador)	Pretty weak (no isotopes measurements for the distal tephra)
	1238B-11H2-82 1238B-10H3-138 1239C-10H3-75	101.22 118.69	**2.18 ± 0.01 Ma**	3–4, diffuse until 8	**5–6**	EC, or CC	WC, EC, or CC	**EC, or CC**	Chacana caldera (Ecuador)	Medium (the tephra composition matches that of Chacana caldera's products, but we are unable to correlate it with a specific proximal deposit)
Late Pliocene	678B-3H3-11 1239A-17H2-85 1238A-14H2-148 1240A-28H1-90	98.47 161.30 133.93 279.95	**2.79 ± 0.01 Ma**	3–6, diffuse until 13	**6**	EC, or CC	EC	**EC**	No volcanoes identified	Isotopic signature close to that of Galeras volcano (Colombia). Proximal deposits

Geochemistry, Geophysics, Geosystems

10.1029/2025GC012278

Table 1
Continued

Epoch	Samples	Top depth of the tephra layer (in mcd)	Age	Thickness of tephra layers (cm)	Estimated VEI	Location of the vent based on geochemistry			Eruptive center that best matches age and geochemistry	Reliability of the correlation and comments
						Major and trace elements	Sr-Pb isotopes	Summary		
										may be part of the Pisayambo formation
	1239A-18H2-120	173.13	**2.89 ± 0.01 Ma**	3	**5–6**	EC	EC, or CC	**EC**	No volcanoes identified	Isotopic signature close to that of Galeras volcano (Colombia). Proximal deposits may be part of the Pisayambo formation
Early Pliocene	1239A-30X1-89	289.90	**3.8 ± 0.2 Ma**	3 (diffuse)	**5–6**	EC	WC, EC, or CC	**EC**	No volcanoes identified	-
	504-38H1-18 1239A-34X5-30	173.00 337.41	**3.9 ± 0.1 Ma**	2	**5–6**	EC	EC, or CC	**EC**	No volcanoes identified	Isotopic signature close to that of Galeras volcano (Colombia). Proximal deposits may be part of the Pisayambo formation
	504-41H1-135 1238A-28X3-123 1239A-37X5-69	187.30 269.15 369.28	**4.3 ± 0.1 Ma**	3–7, diffuse until 35	**5–6**	EC	EC, or CC	**EC**	No volcanoes identified	Isotopic signature close to that of Galeras volcano (Colombia). Proximal deposits may be part of the Pisayambo formation
	677A-23X2-33 1238A-29X3-104 1238A-29X4-43 1239A-40X2-91	203.90 290.66 396.47	**4.8 ± 0.1 Ma**	2–7	**6**	EC	WC, EC, or CC	**EC**	No volcanoes identified	Isotopic signature close to that of Chacana caldera (Ecuador). Proximal deposits may be part of the Pisayambo formation

Note. Column headings indicate geologic epochs, name of tephra samples (composed by site names, hole, core, section, and mean interval; detail of sampling is given in Bablon et al. (2025b)), depth of tephra layers for each site in meters composite depth (mcd; i.e., corrected depth by including sediment gaps), thickness range of tephra layers at all sites, estimated Volcanic Explosivity Index of the eruption (VEI, discussed in Section 4.4, and determined from tephra thicknesses and deposit volume estimates), location of the volcanic source deduced from the geochemical signature of glass shards (WC and EC: Western and Eastern Cordillera in Ecuador; CC: Central Cordillera in Colombia), eruptive centers that present similar geochemistry and whose activity period matches the tephra deposition age, and reliability of this correlation.

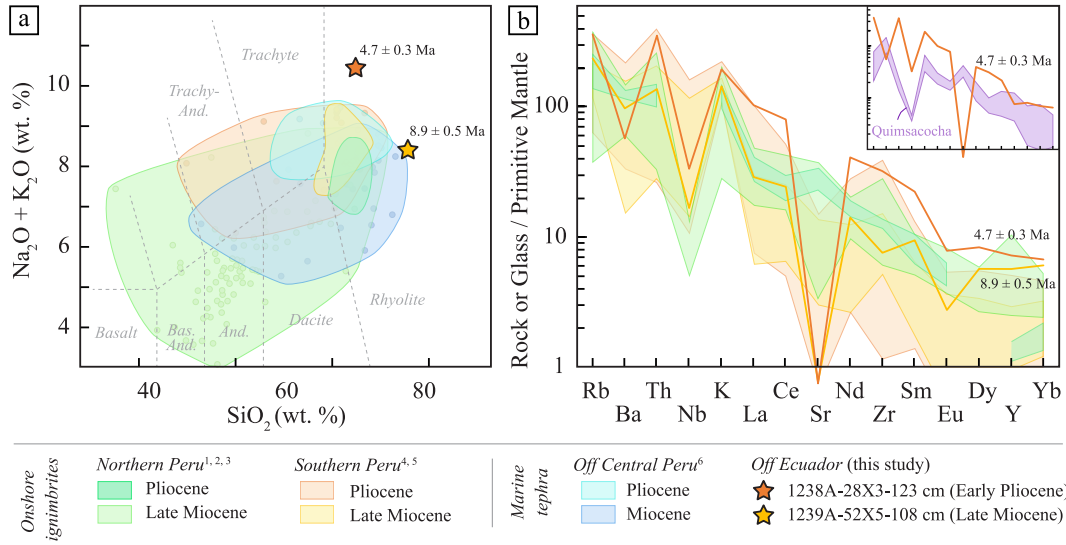

Figure 6. Comparison of the compositions of tephra from the southern part of the Panamá Basin with that of Miocene and Pliocene products of the Peruvian arc. (a) $Na_2O + K_2O$ versus SiO_2 diagram. Colored fields refer to published analyses obtained on products of the currently inactive arc in northern Peru (XRF on whole-rock and unspecified methods, [1] Hollister & Sirvas, 1978, [2] Petford & Atherton, 1994, [3] Rivera et al., 2005), of the Late Miocene and Pliocene ignimbrites of southern Peru (ICP-MS and XRF on whole-rock, [4] Paquereau-Lebti et al., 2006, [5] Mamani et al., 2008). Spider diagrams of incompatible and rare earth elements normalized to primitive mantle (Sun & McDonough, 1989), and of tephra layers sampled in marine sediments off central Peru (Electron microprobe on glass shards, [6] Pouclet et al., 1990). And.: andesite, Bas.: basaltic. (b) Spider diagrams of incompatible and rare earth elements normalized to primitive mantle (Sun & McDonough, 1989). Same legend as (a). No analysis of trace element contents of marine tephra off Peru has been published. The diagram in the insert compares the compositions of the ash emitted at 4.7 ± 0.3 Ma and products of the Mio-Pliocene Quimsacocha caldera located in southern Ecuador (ICP-AES on whole-rock, Beate et al., 2001).

suggesting there is little or no garnet and amphibole in their source (Rivera et al., 2005). Time constraints of volcanic centers and associated deposits are poorly defined, but the composition range of Late Miocene rhyolite products is close to that of the 8.9 ± 0.5 Ma ash sample (Figure 6b), and northern Peru volcanism is the most likely source of this tephra layer. The tephra layer deposited at ***~4.7 Ma***, at Site 1238 exhibits higher alkaline contents (Figure 6a), and a composition significantly different from that of products from the Quimsacocha caldera (Figure 6b), which was active in southern Ecuador during the Early Pliocene. This sample could therefore belong to an eruptive center located in northern Peru, and the associated products are not documented yet. This tephra layer therefore shows that volcanism in this region was active at least until 4.7 Ma, before stopping due to slab flattening.

3.3. Tephra Assigned to the Activity of the Galápagos Hotpot

Five tephra layers have been assigned to the activity of the Galápagos hotpot. The oldest tephra layer has been deposited at ***10.1 ± 0.6 Ma*** and it is the only record of the Galápagos activity identified at Site 1239 (Figure 1). At ODP Site U1381 off Costa Rica, Schindlbeck et al. (2015) identified several tephra layers associated with the Galápagos hotspot between ~16.5 and 8 Ma, with a bimodal, felsic and mafic composition. The geochemical signature of the tephra sampled at Site 1239 is close to that of the described Miocene felsic glass shards (black line and yellow field, respectively, Figure 7a), but it is significantly enriched in LREE compared to tephra of similar age (gray dotted lines, Figure 7a). It exhibits high lead isotopic ratios, close to products from Floreana Island (pink field, Figure 7b), but the oldest known aerial lava was emitted significantly later, at ~1.6 Ma (Harpp et al., 2014; White et al., 1993). Furthermore, the central saddle of the Carnegie Ridge (Figure 1) may result from a southward ridge jump that placed the Galápagos hotspot beneath the Cocos plate between ~14.5 and 7.5 Ma (Barckhausen et al., 2001; Sallarès & Charvis, 2003). This event is associated with an apparent increase in the Galápagos activity and the occurrence of major explosive eruptions (Schindlbeck et al., 2015). Our ~10.1 Ma tephra sample from Site 1239 is coeval with this period of high activity, and may have a source on an old and currently

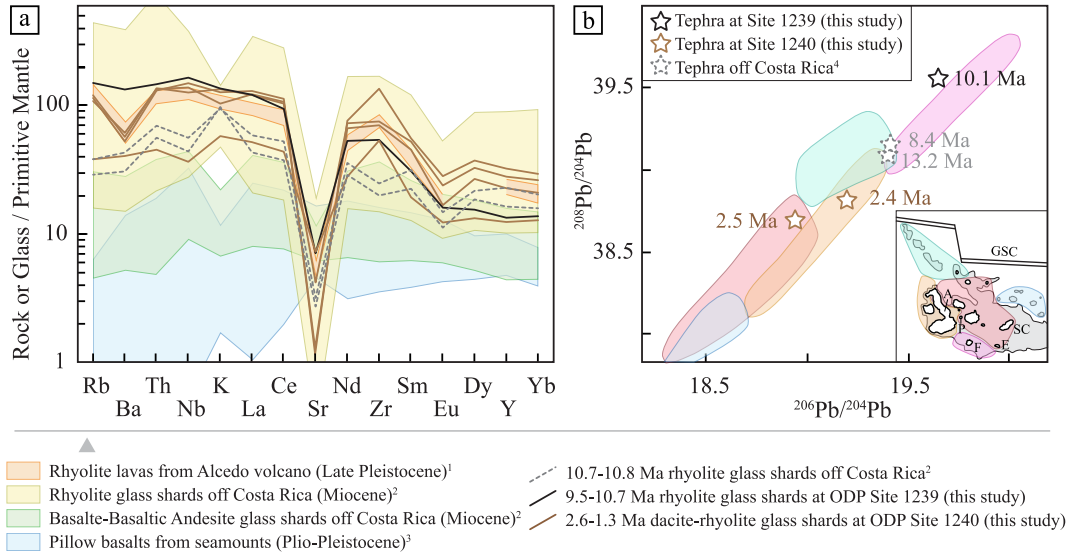

Figure 7. Comparison of the composition of tephra from the southern part of the Panamá Basin with that of products emitted by the Galápagos hotspot. (a) Spider diagrams of incompatible and rare earth elements normalized to primitive mantle (Sun & McDonough, 1989). [1] Whole-rock analyses of rhyolite lavas from Alcedo volcano, on Isabela Island (Geist et al., 1995), [2] Average of LA-ICP-MS measurements obtained on single glass shards of tephra sampled at ODP Site U1381 off Costa Rica (Schindlbeck et al., 2015), [3] ICP-MS measurements performed on whole-rock of dragged rocks from seamounts northeast of the current Galápagos archipelago (Sinton et al., 2018). (b) $^{208}Pb/^{204}Pb$ versus $^{206}Pb/^{204}Pb$ ratios. Volcanic centers associated with colored fields (isotope data from the Georoc database) are represented in the inset map, based on domains defined by Hoernle et al. (2000). [4] MC-ICP-MS measurements of tephra sampled at ODP Site U1381 (Schindlbeck et al., 2015). E, F, P, SC: Española, Floreana, Pinzón and San Cristobal Islands, respectively; A: Alcedo volcano, on Isabela Island; GSC: Galápagos Spreading Center.

dismantled island from the area of the present Floreana Island, since the geochemical zonation in the present-day archipelago is a long-term phenomenon related to inherent plume heterogeneity (Harpp et al., 2005).

No tephra layers from the Galápagos younger than 8 Ma are present at Site U1381 off Costa Rica due to a sedimentary hiatus, nor at Site 1239 off Ecuador. Records in marine sediments take over at Site 1240 with four tephra layers deposited at 2.5 ± 0.1, 2.4 ± 0.1, 2.2 ± 0.1, and 1.36 ± 0.05 Ma (Bablon et al., 2025b). Inferred from geographical reconstructions (e.g., Collot et al., 2009; Meschede & Barckhausen, 2001; Sallarès & Charvis, 2003), the paleoposition of Site 1240 was ~180 km east of Fitzroy and Beagle seamounts (#31 and 32, Figure 1a), which were active and emerged during the Early Pleistocene (Christie et al., 1992; Sinton et al., 2018). However, dated dredged rocks are pillow basalts, which are less enriched in incompatible elements than tephra layers with dacitic to rhyolitic glass compositions due to their lower differentiation degree (blue field and brown lines, respectively, Figure 7a). In addition, they have significantly lower lead isotopic ratios (blue field, Figure 7b; Sinton et al., 2018). Among islands of the current archipelago, only Española and San Cristobal (E and SC in Figure 6b) were active between ~2.6 and 1.3 Ma (Geist et al., 1986; White et al., 1993), and have Pb isotopic ratios close to those of the tephra emplaced at 2.5 ± 0.1 Ma. The geochemical signatures of Quaternary tephra from Site 1240 are similar to that of Miocene tephra identified off Costa Rica (brown lines and yellow field, respectively, Figure 7a; Schindlbeck et al., 2015), supporting that major explosive eruptions occurred until at least 1.3 Ma. These major events could reflect another plume-ridge interplay, as a major southward ridge jump occurred at ~2.6 Ma and placed a segment of the GSC close to the Galápagos plume (Harpp et al., 2005). Unusual rhyolitic lavas were also reported on Pinzón and Alcedo volcanoes (P and A in Figure 6b), and were emplaced during the past ~1 Myr and 100 kyr, respectively (Geist et al., 1995). Contents in incompatible elements of Alcedo's rhyolitic lavas are close to those of Quaternary tephra layers sampled at Site 1239 (orange field and brown lines, respectively, Figure 7a), and their Pb isotopic ratios are similar (red and orange fields, Figure 7b). Geist et al. (1995) inferred that rhyolitic phases occurred when islands were carried away from the focus of the Galápagos hotspot, and are related to the decrease in supply of basaltic magma permitting the magma chamber to cool and evolve by crystallization.

Based on glass shards morphology, we concluded that samples assigned to the activity of the Galápagos hotpot were emplaced during subaerial or quite shallow submarine eruptions, and that the ash emitted at 2.4 ± 0.1 Ma have been likely emplaced close to the vent (Bablon et al., 2025b). Shallow submarine volcanic events can produce subaerial Plinian plumes, depending on mass eruption rates, eruption temperature, vent width and depth (Cahalan & Dufek, 2021). This therefore occurred more frequently during the last construction stages of seamounts, when their summit vent shallowed. Tephra depositional mechanisms might be then sediment gravity flow generated by submarine or subaerial column collapse, or classic sedimentation in the water column after tephra fallout on the sea surface (e.g., Fuller et al., 2018). Since studied tephra layers are lithic-poor and lack quenched shards typical of magma-water interaction, we cannot clearly distinguished whether they were emitted by emerged islands or seamounts. It is necessary to study these tephra at several drilling sites to determine the extent to which the spatial distribution of deposits is controlled by local topography, thus identifying whether eruptive columns were submarine or subaerial.

4. Discussion

4.1. Challenge in Identifying the Volcanic Source of Distal Tephra

The identification of the source of the Pliocene tephra has strong limitations due to the limited knowledge of the spatial organization of the Northern Andean arc and active eruptive centers during the Pliocene. Ash layers recorded in Pliocene coastal sediments north of Ecuador exhibit less differentiated compositions than our Pliocene tephra layers (green field; Figure 2a; Aalto & Miller, 1999), and no analyses of their trace elements nor Sr-Pb isotopy have been reported as far as we know. However, since whole-rock measurements carried out on coastal tephra are dependent on their mineral contents, which are fractionated during transport of particles in the atmosphere (i.e., the distal ash is mainly constituted by glass shards, whereas proximal tephra deposits yield glass shards and phenocrysts), we do not exclude that some tephra layers could be correlated with our samples. In addition, products emitted by the Quimsacocha caldera are significantly more depleted in alkaline and Nb than our Pliocene tephra (purple fields; Figures 2a–2c; Beate et al., 2001). Moreover, few geochemical and geochronological data are available for some eruptive centers of the Quaternary arc (e.g., Chalpatán caldera and Chiles volcano in Ecuador, Nevado del Huila and Cumbal volcanoes in Colombia) and most analysis of on land products were also performed on whole-rock. Our work therefore constitutes a first catalog of explosive events from the Northern Andean arc that have sent products to the Pacific Ocean, but some correlations need further corroboration in the future through new descriptions and analyses of proximal subaerial deposits.

4.2. Temporal Evolution of the Geochemistry of Magmas of the Northern Andes Since the End of the Miocene

Tephra recorded in marine sedimentary sequences allow the study of changes in magma geochemistry on an extended time scale. The temporal evolution of the concentrations in some representative elements in glass shards analyzed in our work is represented in Figure 8. Although it may be biased by the low number of Pliocene eruptions recorded in marine sediments, we observe that ranges of composition of rhyolitic magmas are wider for ash emitted during the past ~1.5 Myr, for many major and trace elements (K_2O, Rb, Nb, Figure 8a; TiO_2, Al_2O_3, FeO, CaO, Ba, Y, MREE and HREE, not shown), and for Pb isotopic ratios ($^{206}Pb/^{204}Pb$, $^{208}Pb/^{204}Pb$, Figures 8a; $^{207}Pb/^{204}Pb$, not shown). In particular, we note that the oldest rhyolitic glass shards exhibit slightly higher K_2O contents and lower Ba/Nb ratios than part of younger Pleistocene shards (Figure 8a). Volcanic centers of the Ecuadorian arc are enriched in incompatible element contents away from the trench, interpreted as mainly resulting from a decrease in the amount of fluids released from the subducting slab, and thus a decrease of partial melting of the mantle wedge (e.g., Ancellin et al., 2017; Barragán et al., 1998; Hidalgo et al., 2012). Consequently, volcanoes located in the Western Cordillera display lower K_2O contents than those located in the Eastern Cordillera, and magmas mainly belong to the low-K calc-alkaline series (e.g., Ancellin et al., 2017). In addition, volcanoes from the Western Cordillera are enriched in fluid-mobile over aqueous fluid-immobile ratios (e.g., Ba/Nb), which may reflect an extensive dehydration of the slab beneath the frontal part of the arc (e.g., Ancellin et al., 2017). Although geochemical models are required to interpret such evolution and quantify slab, mantle wedge, and crust components involved in magma genesis, which is beyond the scope of this paper, the broadening of ranges of major-trace element contents in Pleistocene magmas may reflect the progressive extension of the arc toward the margin, while maintaining sustained activity in the Eastern Cordillera and Sub-andean region. This interpretation is consistent with the regional geology, since no Pliocene deposits have been identified in the

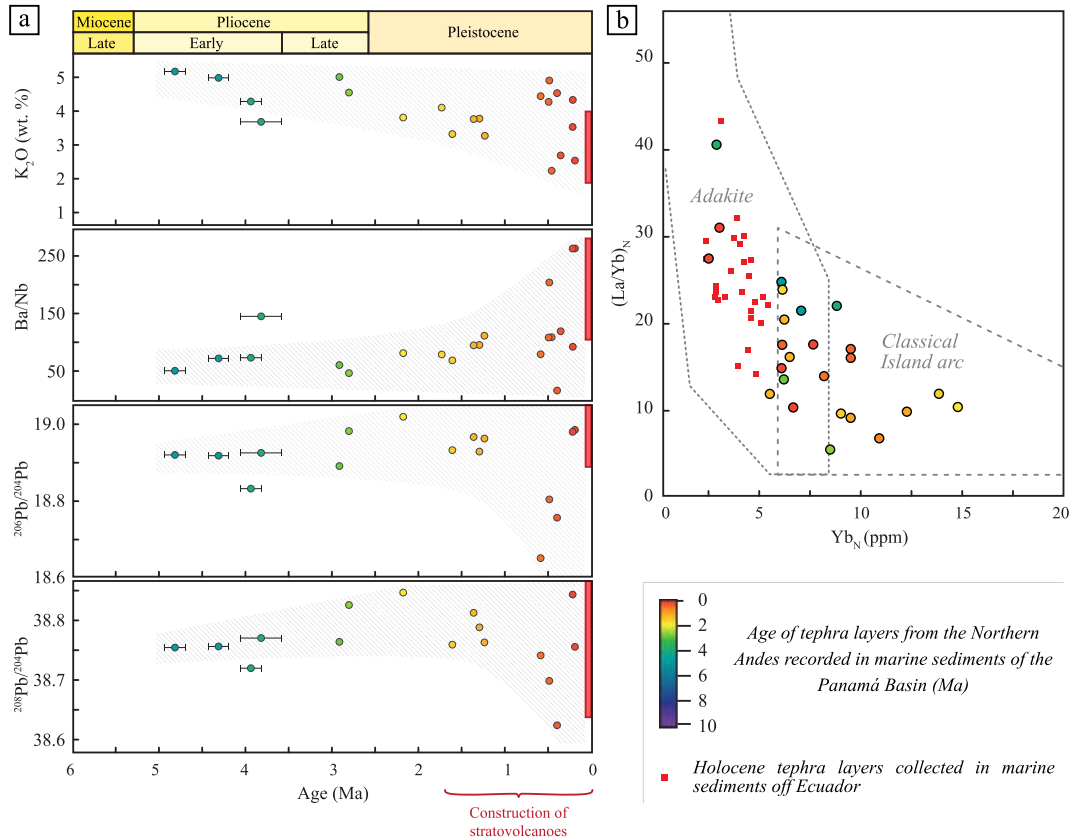

Figure 8. Temporal evolution of the geochemistry of tephra from the Northern Andes since the Late Miocene with dacitic and rhyolitic glass compositions. Values correspond to the average measurements obtained by election microprobe and LA-ICP-MS on single glass shards (Bablon et al., 2025b). (a) Temporal variation of the contents in K_2O, and of Ba/Nb, $^{206}Pb/^{204}Pb$ and $^{208}Pb/^{204}Pb$ ratios in tephra with dacitic and rhyolitic compositions. Samples with andesitic composition (Figure 2a) have been discarded. Hatched gray areas highlight the overall trends of temporal evolution of magma composition. Red rectangles: composition range of Holocene tephra recorded in marine sediments off Ecuador and Colombia (Bablon et al., 2022). (b) Evolution of the La/Yb ratio as a function of the Yb content normalized to chondrites (Sun & McDonough, 1989). Fields of adakites and classical island arc according to Drummond and Defant (1990). Red squares: Holocene tephra recorded in marine sediments (Bablon et al., 2022).

Western Cordillera between 0.5°N and 2°S, whereas products of the Mio-Pliocene Pisayambo Formation largely crop out in the Eastern Cordillera. In addition, this broadening of the composition of rhyolitic magmas is coeval with record of andesitic glass shards in marine sediments (since ~1.6 Ma; Figure 2a), and ages obtained at the arc scale for the construction of stratovolcanoes (Santamaría et al., 2024, and references therein). Although the $^{206}Pb/^{204}Pb$ and $^{208}Pb/^{204}Pb$ ratios of the Western and Eastern Cordillera volcanoes partly overlap (e.g., Ancellin et al., 2017), we also observe wider range values for Pleistocene rhyolitic glass shard (Figure 8a), supporting a greater diversity of magmas from ~1.5 Ma.

Some studies reported an evolution of the geochemical composition of magmas of edifices active over long timespans at the scale of volcanic edifice from typical arc compositions toward adakite-like signatures, such as for Atacazo, Cayambe, Iliniza, Mojanda-Fuya, and Pichincha volcanoes (for products younger than ~70, 400, 50, 500, and 60 ka, respectively; e.g., Hidalgo, 2006; Hidalgo et al., 2007; Robin et al., 2009; Samaniego et al., 2002, 2005, 2010). Adakites are mainly defined by high Al, Na and Sr contents, low Y and HREE contents, resulting in high La/Yb and Sr/Y ratios (Defant & Drummond, 1990; Martin et al., 2005). This may result from the partial melting of a basaltic source leaving a garnet-rich residue, namely the subducted oceanic crust or the lower crust beneath the arc (e.g., Bourdon et al., 2002; Bryant et al., 2006; Chiaradia et al., 2009, 2020; Garrison & Davidson, 2003; Gutscher et al., 2000; Hidalgo et al., 2007; Robin et al., 2009; Samaniego et al., 2005). Following the latter interpretation on a larger timescale, Schütte et al. (2010b) interpreted the increase in Sr and decrease in HREE contents from the Oligocene granitoids to Quaternary arc magmas as reflecting the crustal thickening, and/

or a deeper source in the crust. Furthermore, latitudinal geochemical variations seem to be related to magma-crust interactions at different depths (Chiaradia et al., 2020), or to changes in the slab component composition linked to the decreasing age of the oceanic floor toward the north (Ancellin et al., 2017). Recently, Narváez et al. (2023) reinforced this latter interpretation demonstrating that the hotter thermal regime of the younger crust north of the Grijalva Fracture Zone (GFZ, Figure 1a) allows the subducting slab to partially melt. Consequently, the mantle wedge is dominantly metasomatized by hydrous siliceous melts produced by slab melting (i.e., the slab component is enriched in fluid-immobile elements, with high La/Nb and Th/Nb and low Ba/La ratios, as well as high $^{206}Pb/^{204}Pb$ ratios), whereas it is metasomatized by aqueous fluids released during slab dehydration south of the GFZ, where the crust is older and colder (i.e., the slab component is enriched in fluid-mobile elements, with low La/Nb and Th/Nb and high Ba/La ratios). As we fail to identify the precise location of all the eruptive centers that emitted tephra recorded in marine sediments, we cannot consider the longitudinal and latitudinal variations on the evolution of the composition of magmas. However, considering the overall trend, we note that the oldest rhyolitic glass shards exhibit signatures of classical island arcs, whereas youngest tephra (i.e., 201 ± 10 ka, 190 ± 10 ka, and Holocene tephra layers) display clearer adakitic-like signatures (Figure 8b).

In Central America, changes in the geochemistry of the Costa Rican and Panamanian arc about 45 Ma and over the past 10 Ma, namely shifts from dominantly basaltic to more andesitic compositions, and increases in Pb isotopic ratios and incompatible element contents, were attributed to the subduction of Galápagos tracks (Gazel et al., 2015). We do not report such clear changes in volcanic products of the Northern Andes recorded in deep marine sediments (Figures 4 and 8). In fact, the Central American arc is constructed on a thin, oceanic-like crust, making the slab melting signature easily identifiable, whereas the crust of the Northern Andean arc is significantly thicker and heterogeneous, blurring deep geochemical signatures. Since no primitive basaltic glass shards were recorded in marine sediments, as low-silica lavas rarely produce major explosive eruptions, a high crustal contamination overprinted the primitive signature of magmas. Consequently, we cannot reliably infer the impact of slab versus mantle wedge and crust components involved in the composition of studied tephra.

4.3. Spatial Distribution of Tephra During Major Plio-Pleistocene Eruptions

The spatial distribution of tephra depends on the eruption magnitude, as well as winds and ocean currents direction and speeds. Bablon et al. (2022) interpreted that the lack of tephra layers associated with some major Holocene eruptions in shallow marine sediments along the Ecuadorian margin can also be related to the remobilization of sea-floor sediments during gravitational or tectonic processes, bioturbation by benthic burrowing fauna after tephra deposition, and drilling operations. Products of explosive eruptions in our study area are mostly distributed to the west due to the prevailing winds and ocean currents (Lonsdale, 1977; Ninkovich & Shackleton, 1975). Accordingly, tephra deposits of Northern Andean volcanoes display westerly dispersal patterns (e.g., Hall & Mothes, 2008a; Hidalgo et al., 2008; Thouret et al., 1995), and the most distal fallouts may reach the coastal region and the Pacific Ocean (e.g., Aalto & Miller, 1999; Vallejo Vargas, 2011).

To assess the size of major Plio-Pleistocene eruptions in the Northern Andes we selected four events that occurred at 4.8 ± 0.1, 2.79 ± 0.01, 1.35 ± 0.01 Ma, and 395 ± 10 ka, for which we mapped tentative isopach contour lines (Figure 9), manually delimiting sub-elliptical envelopes of 1, 3 and 6 cm. Tephra layers emplaced during these eruptions have been correlated in sedimentary sequences of at least two drilling sites, and present sharp contacts with sediments that allow to precisely measure their thickness, although these latter may have been biased by ocean currents and bioturbation. The distance between the paleoposition of drilling sites and the Andean arc decreases over time due to the motion of the Nazca plate. Isopach maps of deposits were therefore created by considering the paleoposition of the drilling sites during volcanic events. Indeed, for a similar thickness on a single drilling site, the older tephra layers may correspond to eruptions more powerful than those of younger layers, or were deposited under conditions more favorable to transport and preservation of particles (i.e., strong high-altitude winds, westward non-erosive ocean currents, and no syn- and post-depositional reworking). From these maps, we calculated the volume of ash emitted by each eruption using a single isopach approach for subaerial deposits (Legros, 2000), and two methods based on a distribution of deposits according to exponential and power laws (Bonadonna & Houghton, 2005). Volumes should be considered with caution as we have few control points, only three contour lines, and no proximal thickness data, but results obtained with the three approaches are consistent (Data Set S3). Bulk volumes range from 23 to 27, 38 to 48, 15 to 18, and from 18 to 23 km^3, for the ∼4.8, 2.8, 1.4 and 0.4 Ma events, respectively, which all correspond to VEI-6 eruptions. As a comparison, the total bulk tephra volume deposited during the VEI-7 eruption of Chalupas caldera is estimated at

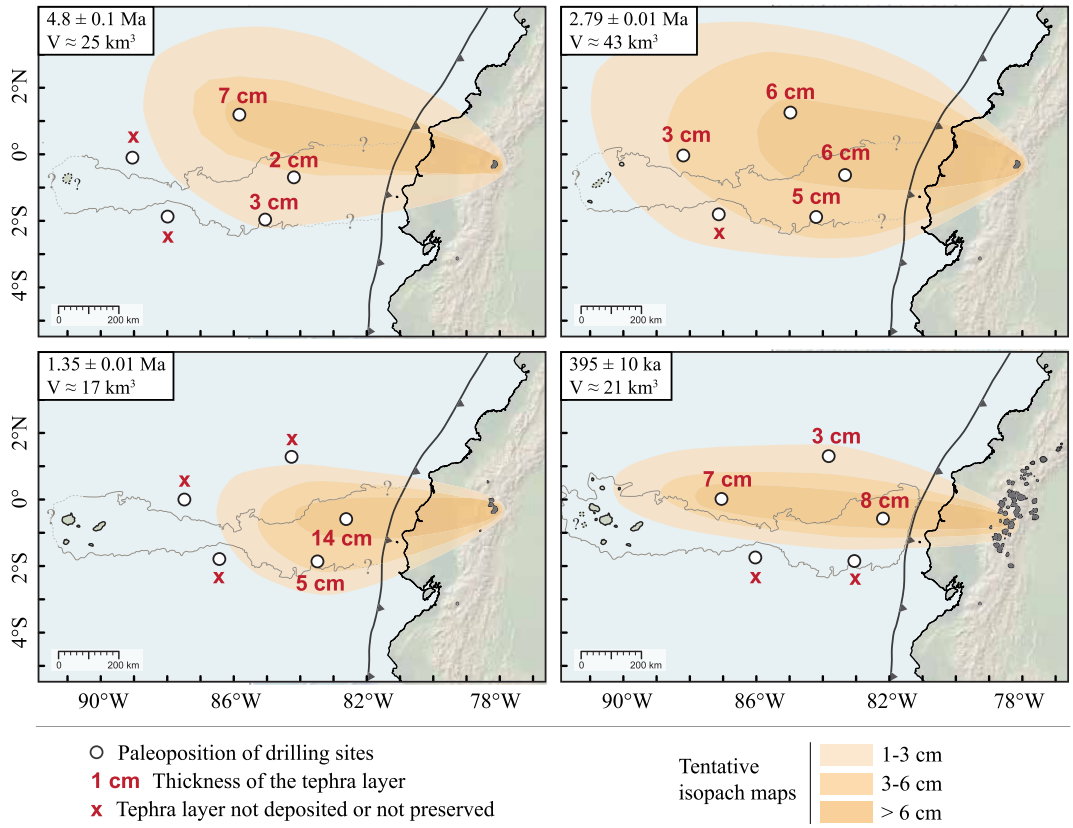

Figure 9. Tentative isopach maps (1, 3 and 6 cm) of four major representative eruptions that occurred at 4.8 ± 0.1, 2.79 ± 0.01, 1.35 ± 0.01 Ma, and 395 ± 10 ka. White points indicate the paleoposition of DSDP and ODP drilling sites (Figure 1a). The mapping of volcanic centers in the Cordillera and of the Galápagos archipelago is subjective, as we do not precisely know the location of spatial distribution of volcanic edifices and emerged islands during the Pliocene. The position of the plume sources is also speculative, but globally coherent with tephra thicknesses and direction of prevailing winds.

~230 km^3 (Bablon, Quidelleur, Siani, et al., 2020), whereas volumes released by major Holocene eruptions, whose most distal products reached the Ecuadorian trench, range from 1 to 6 km^3 and are ranked at a VEI of 5 (Bablon et al., 2022; Vallejo Vargas, 2011). Quilotoa also experienced a VEI-6 explosive event in 1150–1300 cal BCE (Mothes & Hall, 2008), but no tephra layers were identified in marine sediment, due to loss of shallow sediments during coring, sampling bias or strong bottom currents during the eruption (Bablon et al., 2022). Accordingly, apart from the VEI-7 Chalupas eruption, visible tephra recorded in deep-sea sediments result from VEI-5-6 Plinian eruptions (Table 1). Other explosive events of similar magnitude were documented in the Central and Southern Andes, such as the 1600 AD eruption of Huaynaputina volcano in Peru (13–14 km^3, Prival et al., 2020), or the Late Pleistocene-Holocene major eruptions of Hudson volcano in Chile (10–20 km^3, Weller et al., 2015). Smaller explosive eruptions may also have deposited cryptotephras (i.e., glass shards and minerals not visible to the naked eye) in the Panamá Basin, but these microscopic deposits were not studied in this work.

4.4. Eruptive Frequency in the High VEI Range for the Northern Andean Arc Since the Late Miocene: Implications for Regional Geodynamics

The cumulative number of tephra layers from the Northern Andes identified within the Panamá Basin for the past 6 Ma highlights four periods at >5.0, 5.0–3.8, 3.8–3.0 and <3.0 Ma, during which records of major eruptions in marine sediments suggest different eruptive dynamics (red curve, Figure 10), and that we discuss hereafter.

Although biostratigraphy indicates that the deepest sediments recovered at Site 1239 are 15 Ma-old, no tephra from the Northern Andes were identified in the cores for the Middle and Late Miocene (①, Figure 10). Volcanism was active in Ecuador and Colombia during the Miocene, as evidenced by thick volcaniclastic deposits and products from the Quimsacocha caldera in southern Ecuador (Beate et al., 2001; Bernet et al., 2020; Egüez

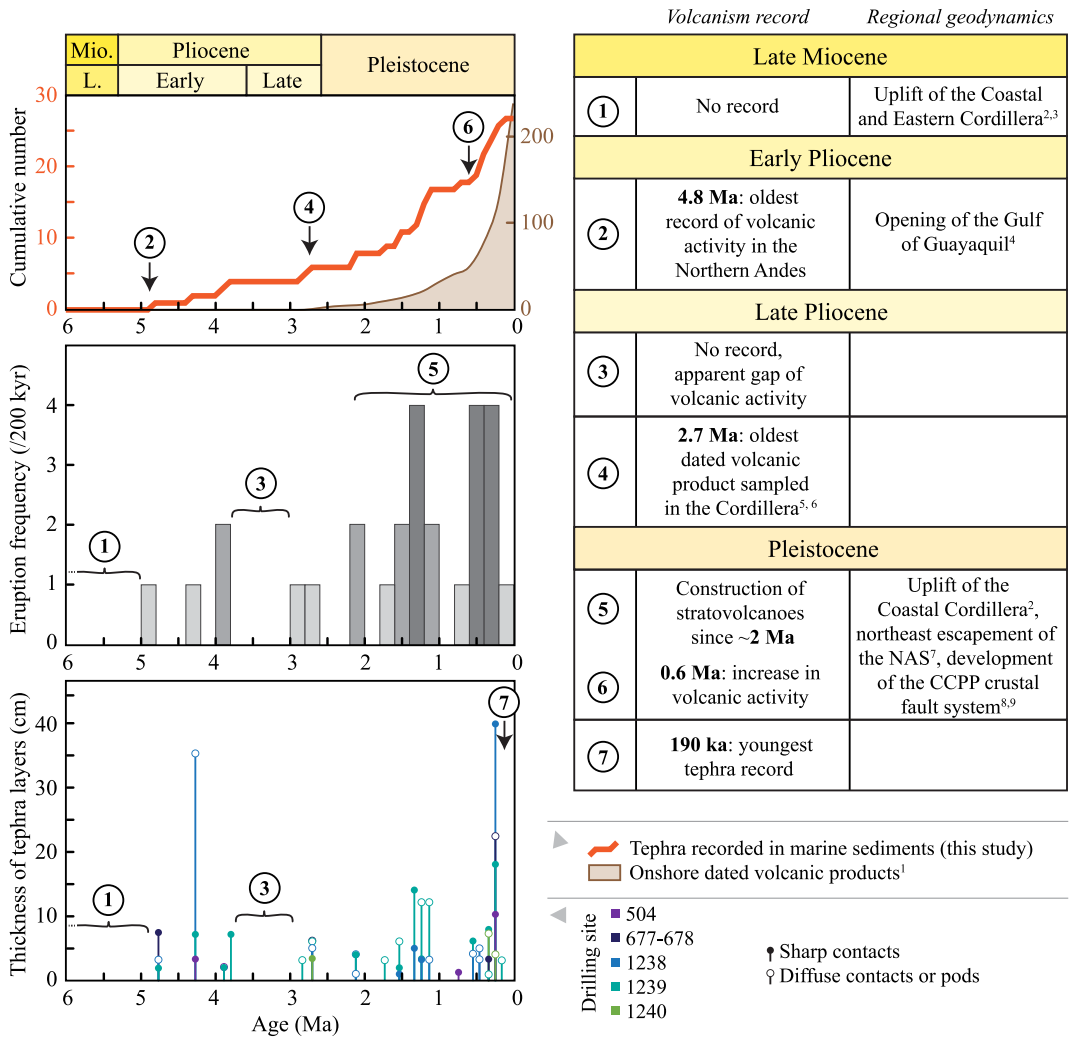

Figure 10. Relationship between the record of the activity of the Northern Andean arc in marine sediments of the southern Panamá Basin and changes in regional geodynamics. Upper graph: the red line represents the cumulative number of tephra layers recorded within deep-sea cores (correlated tephra beds between sites or within a site were counted only once), and the brown line is the cumulative number of K-Ar performed on groundmass, ^{40}Ar/39Ar and fission track ages obtained on Ecuadorian continental volcanic products, calculated with steps of 0.2 Ma. Middle graph: number of tephra layers from the Northern Andes recorded in marine sediments every 0.2 Myr (correlated tephra beds between sites or within a site were counted only once). Lower graph: thickness of tephra layers at each studied drilling site (Figure 1a). [1] Santamaría et al., 2024, and references therein; [2] Brichau et al., 2021; [3] Margirier et al., 2023; [4] Deniaud et al., 1999; [5] Opdyke et al., 2006; [6] Hoffer et al., 2008; [7] Witt et al., 2006; [8] Lavenu et al., 1995; [9] Alvarado et al., 2016.

et al., 2017; Hungerbühler et al., 2002; Schütte et al., 2010a). As mentioned above, the distribution of ash layers in the eastern equatorial Pacific is mainly controlled by the size of the eruption, the volcanic cloud dispersal pattern, and the directions of the ocean currents (Shipboard Scientific Party, 2003). Consequently, the magnitude of Miocene eruptions could have been too small to send ash to the distal studied core areas, or wind flow patterns may have had distributed the ash to other regions, thus explaining their absence in deep-sea sediments studied here. In addition, sediments that were near the coast in the Miocene, and that could have recorded tephra layers, have entered the trench and have been subducted.

The oldest recorded ash was emitted in the beginning of the Early Pliocene (②, Figure 10). During this period, the Ecuadorian Andes already reached high elevations, as supported by pollen records at Site 1239 (i.e., Páramo vegetation, Grimmer et al., 2018), and consistent with exhumation ages inferred from thermochronological data (e.g., Spikings et al., 2001, 2005). Products of four major eruptions were recorded between 4.8 and 3.8 Ma, with a rhyolitic composition close to that of the Chacana caldera. In addition, several ash layers are present in Pliocene

coastal sediments north of Ecuador (Aalto & Miller, 1999). Geochronological studies in the Andean cordillera show that the oldest products from the current arc were emitted in the early Pleistocene. Distal tephra deposits reveal for the first time that the activity of the current arc covers not only the Quaternary, but also Pliocene times. The Pisayambo and Tarqui Formations, composed of andesitic to rhyolitic pyroclastic deposits and lavas, and which crop out in the Eastern Cordillera and south of Ecuador (e.g., Egüez et al., 2017), could correspond to the proximal deposits associated with this eruptive period. Future investigations could focus on these deposits that have received little attention so far, in order to better characterize the early construction stages of the current arc and identify if 4.8 Ma corresponds to a progressive switch over of the activity from southern to northern Ecuador.

This period is followed by about 1 Myr without any known volcanic record (③, Figure 10). This apparent gap could be explained by a decrease in strength and/or a change in direction of prevailing winds, an increase in strength of regional ocean currents, or a significant decrease in the frequency of high magnitude eruptions onland. However, Steph et al. (2010) related the increase of coastal upwelling and biogenic productivity of the eastern equatorial Pacific to strengthening of the trade winds since ∼3.6–3.5 Ma. A 1 Myr period with minor volcanic activity could induce a progressive erosion of older, uncovered volcanic deposits, which could explain why the oldest product of the current arc is dated at 2.7 Ma in the cordillera (④, Figure 10).

From 2.9 Ma the volcanic activity resumed, with an increase in frequency of records in marine sediments since ∼2 Ma (⑤, Figure 10). This apparent increase may be biased by the convergence of the Nazca plate, and thus by the reduction of the distance between the paleoposition of drilling sites and the volcanic vents through time (Figure 1a). However, geochronological studies carried out in the past three decades also demonstrated that the volcanic activity actually intensified (brown curve, Figure 10), accompanied by the gradual increase of the number of active eruptive centers (e.g., Santamaría et al., 2024). In addition, in the coastal plain of Ecuador, the Santo Domingo alluvial megafan drained erosion products from catchments of the cordillera (Reyes, 2013). These erosion products lie on the Plio-Pleistocene Borbón Formation and were syn- and post-deposition deformed by a Pleistocene uplift of the Coastal Cordillera (Hernández et al., 2024; Reyes, 2013), which coincides with the ∼2 Ma exhumation pulse identified by Brichau et al. (2021). Despite the lack of available geochronological data on volcaniclastic products of the Santo Domingo fan, the important imput flux of sedimentary and volcaniclastic material supplied to the fan also evidence an increase of the volcanic activity from the Early Pleistocene. No tephra layers were recorded from ∼2.8 to 2.2 Ma (Figure 10), which may be related to strong bottom currents that eroded deep-sea sediments south of the Carnegie Ridge at the Pliocene-Pleistocene boundary (Michaud et al., 2018).

The composition of magma of major eruptions becomes more diversified from ∼2 Ma, with the emission of dacite and andesite ash (e.g., Figure 8), which may reflect the beginning of the construction of stratovolcanoes, whereas large rhyolitic eruptions still occurred. However, no products assigned to this early activity of stratovolcanoes have been dated in the Cordillera. From ∼1.5 Ma, some tephra layers exhibit lower K_2O and incompatible element contents, and were likely associated with the early construction of volcanic edifices in the Western Cordillera, consistent with the age of onland dated products (1.29 ± 0.01 and 1.11 ± 0.02 Ma for Atacazo and Pichincha volcanoes, respectively, Hidalgo, 2006; Robin et al., 2010). Geochronological study of proximal products highlights a northward and southward extension of the volcanic activity in Ecuador from ∼600 ka (⑥, Figure 10; Bablon, Quidelleur, Samaniego, et al., 2020; Bablon et al., 2019; Santamaría et al., 2024). This arc development is also evidenced, to a lesser extent, by an increase in the number of tephra layers in marine archives (⑦, Figure 10). The last VEI-5-6 eruption recorded in deep-sea sediments occurred at 190 ka. However, the "Pifo" pumice fall layer, a key stratigraphic marker of the northern Ecuadorian arc (Hall & Mothes, 1997; Robin et al., 2009), sourced at the Chacana caldera between 220 ± 20 and 150 ± 20 ka (Bigazzi et al., 1992; Hall & Mothes, 1997), was not identified from compositional constraints at any of the studied sites.

The spatial distribution of volcanic edifices from the Northern Andean arc seems to be guided by several factors including deep mechanisms (i.e., slab geometry and age, mantle heterogeneities), crustal tectonic structures, and Quaternary tectonic activity, whereas the thermal regime anomaly of the subducting young Nazca crust and the Carnegie Ridge may have major control on magma genesis (e.g., Bablon, Quidelleur, Samaniego, et al., 2020; Barberi et al., 1988; Santamaría et al., 2024).We propose two models to integrate our data to the understanding of the long-term evolution of the regional geodynamics (Figure 11). For both models, we assume that the convergence velocity of ∼6 cm/yr of the Nazca Plate (e.g., Nocquet et al., 2014) is almost constant since the Early Pliocene (Schütte et al., 2010a, Schütte et al., 2010b), and that the time interval between the release of fluids from

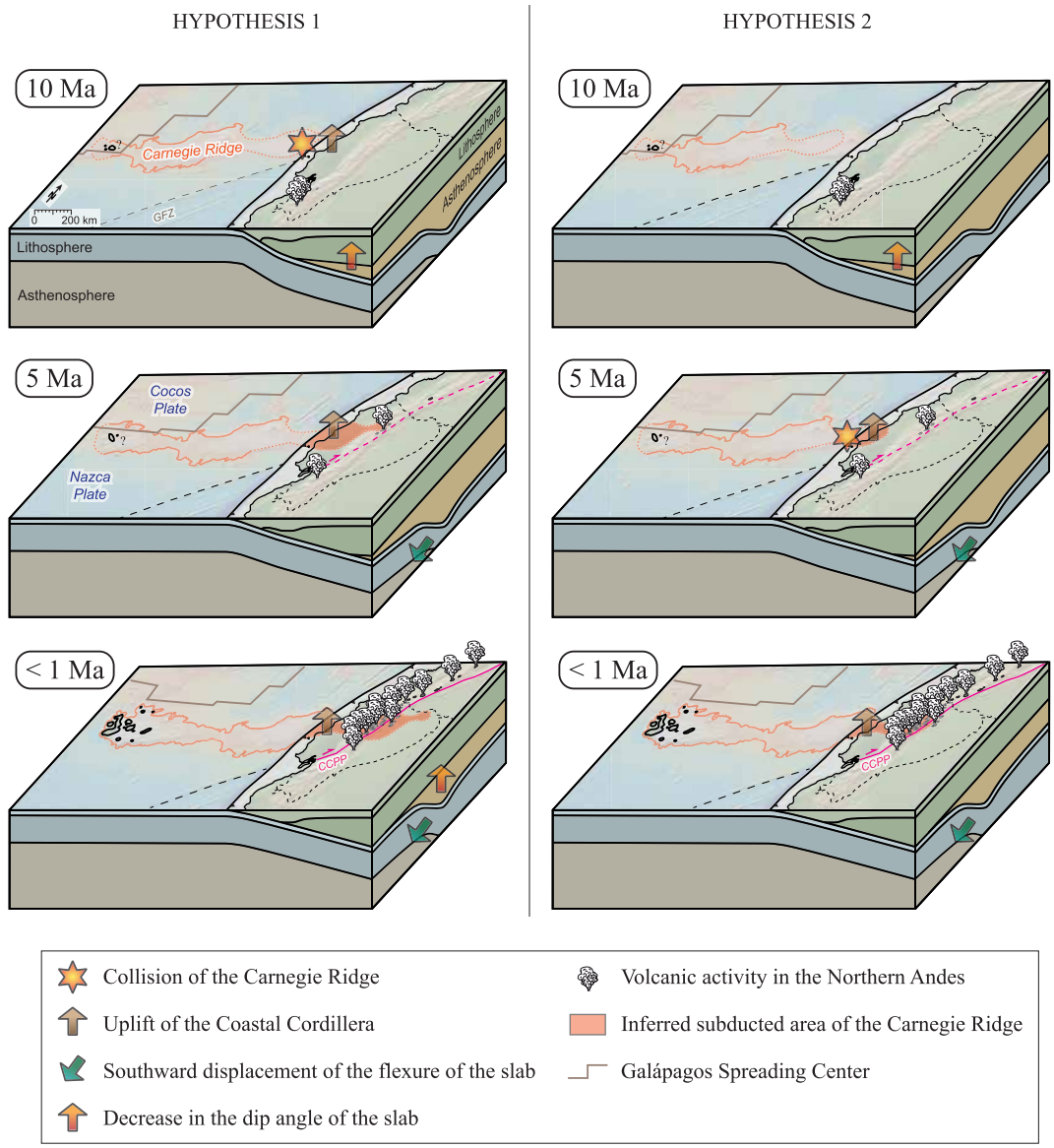

Figure 11. Models of geodynamic reconstructions of the northern Andes during the past 10 Myr. GFZ: Grijalva Fracture Zone, CCPP: Chingual-Cosanga-Pallatanga-Puná fault system. Note that we only represented active volcanoes whose products were identified on land or in marine sediments, but we do not exclude that other volcanic centers were active between 10 and 5 Ma.

the slab and the eruption is a few hundred kyr or even less (e.g., Ruprecht & Plank, 2013; Sigmarsson et al., 1990; Turner et al., 2000; Vlastélic et al., 2023).

In the first hypothesis, the Carnegie Ridge could have started to subduct about 10 Myr ago, triggering the first exhumation pulse identified in the Coastal Cordillera at ~8–10 Ma (Brichau et al., 2021). The tip of the ridge arrived under the Andes at ~5 Ma (i.e., after 5 Myr to cover the ~300 km between the trench and the sub-arc area), triggering magma genesis and explosive rhyolitic volcanism near 0° latitude. The lack of tephra records between 4 and 3 Ma (Figure 10) may be associated with a narrow part of the Carnegie Ridge below the Cordillera, illustrating a ridge jump above the Galápagos hotspot at ~14 Ma (Sallarès & Charvis, 2003). At 5 Ma, a larger part of the Carnegie Ridge may have started to subduct, coeval with a second uplift of the Coastal Cordillera (Brichau et al., 2021). This larger part has arrived below the Cordillera, and may have initiated a decrease of the subducted slab angle, leading to an increase in slab dehydration and magma genesis, widening of the arc near 0° latitude, and

diversified magma compositions. This model is consistent with paleogeographic reconstructions (Daly, 1989) and exhumation ages of this part of the Andes (Spikings et al., 2001, 2005).

In the second hypothesis, the Carnegie Ridge could have started subducting later, at about 5 Ma, coeval with the second exhumation pulse identified by Brichau et al. (2021) in the Coastal Cordillera, and the most recent uplift identified in the Eastern Cordillera (Margirier et al., 2023). This age is also in agreement with the submarine morphological markers of the margin (Collot et al., 2009). In that case, the oldest exhumation pulse of the Coastal Cordillera at ∼8–10 Ma (Brichau et al., 2021) may represent subduction of another older sea-floor asperity. At 5 Ma, volcanism was active in the Cordillera, and represented a more classical subduction activity. The increase of the velocity of escapement of the NAS and the most recent uplift of the Coastal Cordillera ∼2 Myr ago (e.g., Brichau et al., 2021; Witt et al., 2006) may reflect the subduction of a wider part of the ridge. Considering the current ∼6 cm/yr velocity of the Nazca plate, the extremity of the ridge reached the sub-arc area during the past ∼1.5 Myr, favoring slab dehydration and melting, and explaining the recent intensification of volcanic activity, as well as the geochemical changes of Late Pleistocene-Holocene magmas (Figure 8). In addition, the (re)activation of the crustal faults since the end of the Pliocene (e.g., Alvarado et al., 2016) may have influenced the widening of the arc. This hypothesis may be most probable, as it is consistent with paleogeographic reconstructions of the Ecuadorian margin (Collot et al., 2009, 2019).

The lack of temporal constraints for the development of the CCPP fault system prevents understanding the relationship between the volcanic and tectonic activities. Similarly, the eruptive history of many volcanoes in Colombia is poorly known. As their construction was not controlled by the subduction of the Carnegie Ridge, geochronological data would be essential to compare the geochemistry and development of a volcanic arc with or without the subduction of an oceanic ridge in this region. Future investigations should therefore focus on these mechanisms in order to identify more reliably the most likely geodynamic evolution for the Northern Andes.

5. Conclusion

Based on the age models, geochemical analyzes and isotopic data of ash emitted by 34 explosive eruptions during the past 10 Myr and recorded in marine sediments of the Panamá Basin (Bablon et al., 2025b), we propose models of the long-term evolution of the volcanic activity in the Northern Andes. Volcanism was active in northern Peru-southern Ecuador at least between ∼8.9 and 4.7 Ma, before stopping due to the decrease in the slab dip angle. The oldest known deposits of explosive volcanic activity in northern Ecuador-southern Colombia were emplaced ∼4.8 Ma ago. Four tephra layers were identified in Pliocene sediments and correspond to large rhyolitic explosive events that likely occurred in the Eastern Cordillera of Ecuador. After a ∼1 Myr apparent gap of activity, frequencies of records increased from the end of the Pliocene. During this period, broader ranges of values of major-trace element contents of magmas seemingly coincides with maturation of the arc that includes the construction of stratovolcanoes, the progressive widening of the arc during the Quaternary, and with the subduction of the young oceanic Nazca plate and the Carnegie Ridge near the Equator. Future investigations focusing on the Colombian volcanism north of the Carnegie Ridge and on Mio-Pliocene Formations in Ecuador providing time constraints to the development of regional faults and volcanism is crucial to decipher the role of such deep and shallow processes on the spatial and temporal development of volcanic arcs in subduction contexts.

Data Availability Statement

The location of coring sites, depth of tephra layers, as well as raw electron microprobe, LA-ICP-MS, ICP-AES and MC-ICP-MS data are archived and available at Zenodo data repository via Bablon et al. (2025a).

Acknowledgments
The authors are grateful to an anonymous reviewer for its suggestions and constructive comments that helped us to improve this manuscript, and to Marie Edmonds for the editorial handling. This study is part of the ANR MARACAS program (ANR-18-CE31-0022, PI: M. Saillard), and of the Laboratoire Mixte International "Séismes et Volcans dans les Andes du Nord" program, an Ecuadorian-French cooperation program between the IG-EPN and the French National Research Institute for Sustainable Development (IRD). Mathilde Bablon benefited from the valuable support of IODP France, whose funding ("Soutien Expéditions Anciennes" 2022) and post-doctoral fellowship made this work possible. CCMA electron microscopy equipment was funded by Région Sud - Provence-Alpes-Côte d'Azur, the Conseil Départemental des Alpes-Maritimes, and the GIS-IBiSA. This is contribution number 719 of the ClerVolc Program of the International Research Center for Disaster Sciences and Sustainable Development of the University of Clermont Auvergne.

References

Aalto, K. R., & Miller, W. (1999). Sedimentology of the Pliocene Upper Onzole formation, an inner-trench slope succession in northwestern Ecuador. *Journal of South American Earth Sciences*, *12*(1), 69–85. https://doi.org/10.1016/S0895-9811(99)00005-X

Almeida Vaca, M., Bablon, M., Andrade, S. D., Hidalgo, S., Quidelleur, X., Vasconez, F. J., et al. (2023). New geological and geochronological constraints on the evolution of the Cotacachi - Cuicocha volcanic complex (Ecuador). *Journal of South American Earth Sciences*, *128*, 104489. https://doi.org/10.1016/j.jsames.2023.104489

Alvarado, A., Audin, L., Nocquet, J. M., Jaillard, E., Mothes, P., Jarrín, P., et al. (2016). Partitioning of oblique convergence in the Northern Andes subduction zone: Migration history and the present-day boundary of the North Andean Sliver in Ecuador. *Tectonics*, *35*(5), 1048–1065. https://doi.org/10.1002/2016TC004117

Alvarado, A., Audin, L., Nocquet, J. M., Lagreulet, S., Segovia, M., Font, Y., et al. (2014). Active tectonics in Quito, Ecuador, assessed by geomorphological studies, GPS data, and crustal seismicity. *Tectonics*, *33*(2), 67–83. https://doi.org/10.1002/2012TC003224

Alvarez Silva, J. D. (2022). *Análisis litofacial y composicional de la Formación Guacacallo al SW del departamento del Huila (Colombia)* (PhD Thesis). Universidad de Caldas Facultad de Ciencias Exactas y Naturales Programa de Geología, Manizales.

Ancellin, M.-A., Samaniego, P., Vlastélic, I., Nauret, F., Gannoun, A., & Hidalgo, S. (2017). Across-arc versus along-arc Sr-Nd-Pb isotope variations in the Ecuadorian volcanic arc. *Geochemistry, Geophysics, Geosystems*, *18*(3), 1163–1188. https://doi.org/10.1002/2016GC006679

Andrade, S. D., Müller, A. V., Vasconez, F. J., Beate, B., Aguilar, J., & Santamaría, S. (2021). Pululahua dome complex, Ecuador: Eruptive history, total magma output and potential hazards. *Journal of South American Earth Sciences*, *106*, 103046. https://doi.org/10.1016/j.jsames.2020.103046

Armijos Vargas, W. G., & Sánchez Pontón, Á. A. (2018). *Estudio de caracterización vulcanológica y petrográfica de las ignimbritas de la Formación Jubones en el sector de Santa Isabel - El Progreso* (Engineer thesis). Escuela Superior Politécnica del Litoral, Guayaquil, Ecuador.

Bablon, M. (2018). *Reconstruction de l'histoire des volcans de l'arc équatorien: contraintes pour l'évolution chronologique de l'arc andin et pour l'évaluation du risque volcanique* (PhD Thesis). University Paris-Sud, Université Paris-Saclay, France.

Bablon, M., Nauret, F., Saillard, M., Samaniego, P., Vlastélic, I., Hidalgo, S., et al. (2023). An innovative isotopic method to identify the volcanic source of distal tephra. *Earth and Planetary Science Letters*, *619*, 118283. https://doi.org/10.1016/j.epsl.2023.118283

Bablon, M., Quidelleur, X., Samaniego, P., Le Pennec, J.-L., Audin, L., Jomard, H., et al. (2019). Interactions between volcanism and geodynamics in the southern termination of the Ecuadorian arc. *Tectonophysics*, *751*, 54–72. https://doi.org/10.1016/j.tecto.2018.12.010

Bablon, M., Quidelleur, X., Samaniego, P., Le Pennec, J.-L., Lahitte, P., Liorzou, C., et al. (2018). Eruptive chronology of Tungurahua volcano (Ecuador) revisited based on new K-Ar ages and geomorphological reconstructions. *Journal of Volcanology and Geothermal Research*, *357*, 378–398. https://doi.org/10.1016/j.jvolgeores.2018.05.007

Bablon, M., Quidelleur, X., Samaniego, P., Le Pennec, J.-L., Santamaría, S., Liorzou, C., et al. (2020). Volcanic history reconstruction in northern Ecuador: Insights for eruptive and erosion rates on the whole Ecuadorian arc. *Bulletin of Volcanology*, *82*(1), 11. https://doi.org/10.1007/s00445-019-1346-1

Bablon, M., Quidelleur, X., Siani, G., Samaniego, P., Le Pennec, J.-L., Nouet, J., et al. (2020). Glass shard K-Ar dating of the Chalupas caldera major eruption: Main Pleistocene stratigraphic marker of the Ecuadorian volcanic arc. *Quaternary Geochronology*, *57*, 101053. https://doi.org/10.1016/j.quageo.2020.101053

Bablon, M., Ratzov, G., Nauret, F., Samaniego, P., Michaud, F., Saillard, M., et al. (2022). Holocene marine tephra offshore Ecuador and southern Colombia: First trench-to-arc correlations and implication for magnitude of major eruptions. *Geochemistry, Geophysics, Geosystems*, *23*(9), e2022GC010466. https://doi.org/10.1029/2022GC010466

Bablon, M., Saillard, M., Michaud, F., Nauret, F., Samaniego, P., Le Pennec, J.-L., et al. (2025a). Geochemical analyses of marine tephra layers collected offshore Ecuador during the DSDP Leg 69 and ODP Legs 111 and 202 [Dataset]. *Zenodo*. https://doi.org/10.5281/zenodo.16088330

Bablon, M., Saillard, M., Michaud, F., Nauret, F., Samaniego, P., Le Pennec, J.-L., et al. (2025b). Offshore record of explosive volcanic eruptions in the southern part of the Panamá Basin During the past 10 Myr (DSDP site 504, ODP sites 677, 678, 1238, 1239, 1240): 1. Tephrostratigraphy, cross-correlations and geochemical characterization.

Barberi, F., Coltelli, M., Ferrara, G., Innocenti, F., Navarro, J. M., & Santacroce, R. (1988). Plio-quaternary volcanism in Ecuador. *Geochemical Magazine*, *125*, 1–14. https://doi.org/10.1017/s0016756800009328

Barckhausen, U., Ranero, C. R., Von Huene, R., Cande, S. C., & Roeser, H. A. (2001). Revised tectonic boundaries in the Cocos Plate off Costa Rica: Implications for the segmentation of the convergent margin and for plate tectonic models. *Journal of Geophysical Research*, *106*(B9), 19207–19220. https://doi.org/10.1029/2001JB000238

Barragán, R., Geist, D., Hall, M., Larson, P., & Kurz, M. (1998). Subduction controls on the compositions of lavas from the Ecuadorian Andes. *Earth and Planetary Science Letters*, *154*(1–4), 153–166. https://doi.org/10.1016/S0012-821X(97)00141-6

Beate, B., Monzier, M., Spikings, R., Cotten, J., Silva, J., Bourdon, E., & Eissen, J. P. (2001). Mio-Pliocene adakite generation related to flat subduction in southern Ecuador: The Quimsacocha volcanic center. *Earth and Planetary Science Letters*, *192*(4), 561–570. https://doi.org/10.1016/s0012-821x(01)00466-6

Béguelin, P., Chiaradia, M., Beate, B., & Spikings, R. (2015). The Yanaurcu volcano (Western Cordillera, Ecuador): A field, petrographic, geochemical, isotopic and geochronological study. *Lithos*, *218–219*, 37–53. https://doi.org/10.1016/j.lithos.2015.01.014

Bellver-Baca, M. T., Chiaradia, M., Beate, B., Béguelin, P., Deriaz, B., Mendez-Chazarra, N., & Villagómez, D. (2020). Geochemical evolution of the Quaternary Chachimbiro volcanic complex (frontal volcanic arc of Ecuador). *Lithos*, *356–357*, 105237. https://doi.org/10.1016/j.lithos.2019.105237

Bernard, B., Hidalgo, S., Robin, C., Beate, B., & Quijozaca, J. (2014). The 3640–3510 BC rhyodacite eruption of Chachimbiro compound volcano, Ecuador: A violent directed blast produced by a satellite dome. *Bulletin of Volcanology*, *76*(9), 849. https://doi.org/10.1007/s00445-014-0849-z

Bernet, M., Mesa Garcia, J., Chauvel, C., Ramírez Londoño, M. J., & Marín-Cerón, M. I. (2020). Thermochronological, petrographic and geochemical characteristics of the Combia Formation, Amagá basin, Colombia. *Journal of South American Earth Sciences*, *104*, 102897. https://doi.org/10.1016/j.jsames.2020.102897

Bigazzi, G., Coltelli, M., Hadler, N. J. C., Araya, A. M. O., Oddone, M., & Salazar, E. (1992). Obsidian-bearing lava flows and pre-Columbian artifacts from the Ecuadorian Andes: First new multidisciplinary data. *Journal of South American Earth Sciences*, *6*(1–2), 21–32. https://doi.org/10.1016/0895-9811(92)90014-P

Bonadonna, C., & Houghton, B. F. (2005). Total grain-size distribution and volume of tephra-fall deposits. *Bulletin of Volcanology*, *67*(5), 441–456. https://doi.org/10.1007/s00445-004-0386-2

Bourdon, E., Eissen, J.-P., Gutscher, M.-A., Monzier, M., Samaniego, P., Robin, C., et al. (2002). Slab melting and slab melt metasomatism in the northern Andean volcanic zone: Adakites and high-Mg andesites from Pichincha volcano (Ecuador). *Bulletin de la Societe Geologique de France*, *173*(3), 195–206. https://doi.org/10.2113/173.3.195

Brichau, S., Reyes, P., Gautheron, C., Hernández, M. J., Michaud, F., Leisen, M., et al. (2021). First timing constraints on the Ecuadorian Coastal Cordillera exhumation: Geodynamic implications. *Journal of South American Earth Sciences*, *105*, 103007. https://doi.org/10.1016/j.jsames.2020.103007

Bryant, J. A., Yogodzinski, G. M., Hall, M. L., Lewicki, J. L., & Bailey, D. G. (2006). Geochemical constraints on the origin of volcanic rocks from the Andean Northern Volcanic Zone, Ecuador. *Journal of Petrology*, *47*(6), 1147–1175. https://doi.org/10.1093/petrology/egl006

Bustos, E., Arnosio, M., Murcia, H., Arango Palacio, E., & Gómez-Vasconcelos, M. G. (2023). Volcanic evolution through geomorphological mapping: A case study of Cerro Bravo volcano (Colombia). *Journal of South American Earth Sciences*, *128*, 104472. https://doi.org/10.1016/j.jsames.2023.104472

Cahalan, R. C., & Dufek, J. (2021). Explosive submarine eruptions: The role of condensable gas jets in underwater eruptions. *JGR Solid Earth*, *126*(2), e2020JB020969. https://doi.org/10.1029/2020JB020969

Calvache, M. L., Cortés J, G. P., & Williams, S. N. (1997). Stratigraphy and chronology of the Galeras volcanic complex, Colombia. *Journal of Volcanology and Geothermal Research*, *77*(1–4), 5–19. https://doi.org/10.1016/S0377-0273(96)00083-2

Cantalamessa, G., & Di Celma, C. (2004). Origin and chronology of Pleistocene marine terraces of Isla de la Plata and of flat, gently dipping surfaces of the southern coast of Cabo San Lorenzo (Manabì, Ecuador). *Journal of South American Earth Sciences*, *16*(8), 633–648. https://doi.org/10.1016/j.jsames.2003.12.007

Ceballos–Hernández, J. A., Martínez–Tabares, L. M., Valencia–Ramírez, L. G., Pulgarín–Alzate, B. A., Correa–Tamayo, A. M., & Narváez–Marulanda, B. L. (2020). Chapter 7. In J. Gómez & A. O. Pinilla–Pachon (Eds.), *The geology of Colombia, volume 4 Quaternary. Servicio Geológico Colombiano, Publicaciones Geológicas Especiales*. https://doi.org/10.32685/pub.esp.38.2019.07

Chiaradia, M., Bellver-Baca, M. T., Valverde, V., & Spikings, R. (2021). Geochemical and isotopic variations in a frontal arc volcanic cluster (Chachimbiro-Pulumbura-Pilavo-Yanaurcu, Ecuador). *Chemical Geology*, *574*, 120240. https://doi.org/10.1016/j.chemgeo.2021.120240

Chiaradia, M., Müntener, O., & Beate, B. (2020). Effects of aseismic ridge subduction on the geochemistry of frontal arc magmas. *Earth and Planetary Science Letters*, *531*, 115984. https://doi.org/10.1016/j.epsl.2019.115984

Chiaradia, M., Müntener, O., Beate, B., & Fontignie, D. (2009). Adakite-like volcanism of Ecuador: Lower crust magmatic evolution and recycling. *Contributions to Mineralogy and Petrology*, *158*(5), 563–588. https://doi.org/10.1007/s00410-009-0397-2

Christie, D. M., Duncan, R. A., McBirney, A. R., Richards, M. A., White, W. M., Harpp, K. S., & Fox, C. G. (1992). Drowned islands downstream from the Galapagos hotspot imply extended speciation times. *Nature*, *355*(6357), 246–248. https://doi.org/10.1038/355246a0

Collot, J.-Y., Michaud, F., Alvarado, A., Marcaillou, B., Sosson, M., Ratzov, G., et al. (2009). Visión general de la morfología submarina del margen convergente de Ecuador-Sur de Colombia: Implicaciones sobre la transferencia de masa y la edad de la subducción de la Cordillera de Carnegie. Geología y Geofísica Marina y Terrestre del Ecuador desde la costa continental hasta las Islas Galápagos. In *Comisión Nacional del Derecho del Mar (CNDM)* (pp. 47–74). Primera Edición.

Collot, J.-Y., Ratzov, G., Silva, P., Proust, J.-N., Migeon, S., Hernandez, M.-J., et al. (2019). The Esmeraldas canyon: A helpful marker of the Pliocene-Pleistocene tectonic deformation of the North Ecuador-southwest Colombia convergent margin. *Tectonics*, *38*(8), 3140–3166. https://doi.org/10.1029/2019TC005501

Córdova, M. D., Mothes, P. A., Gaunt, H. E., & Salgado, J. (2020). Post-caldera eruptions at Chalupas Caldera, Ecuador: Determining the timing of lava dome collapse, hummock emplacement and dome rejuvenation. *Frontiers of Earth Science*, *8*, 548251. https://doi.org/10.3389/feart.2020.548251

Daly, M. C. (1989). Correlations between Nazca/Farallon Plate kinematics and forearc basin evolution in Ecuador. *Tectonics*, *8*(4), 769–790. https://doi.org/10.1029/TC008i004p00769

Davidson, J. P., McMillan, N. J., Moorbath, S., Wörner, G., Harmon, R. S., & Lopez-Escobar, L. (1990). The Nevados de Payachata volcanic region (18∼ S/69∼ W, N. Chile) II. Evidence for widespread crustal involvement in Andean magmatism. *Contributions to Mineralogy and Petrology*, *105*(4), 412–432. https://doi.org/10.1007/bf00286829

Defant, M. J., & Drummond, M. S. (1990). Derivation of some modern arc magmas by melting of young subducted lithosphere. *Nature*, *347*(6294), 662–666. https://doi.org/10.1038/347662a0

Deniaud, Y., Baby, P., Basile, C., Ordoñez, M., Montenegro, G., & Mascle, G. (1999). Opening and tectonic and sedimentary evolution of the Gulf of Guayaquil: Neogene and Quaternary fore-arc basin of the south Ecuadorian Andes. *Acad. Sc. Paris*, *328*(3), 181–187. https://doi.org/10.1016/s1251-8050(99)80094-9

Droux, A., & Delaloye, M. (1996). Petrography and geochemistry of Plio-Quaternary calc-alkaline volcanoes of Southwestern Colombia. *Journal of South American Earth Sciences*, *9*(1–2), 27–41. https://doi.org/10.1016/0895-9811(96)00025-9

Drummond, M. S., & Defant, M. J. (1990). A model for Trondhjemite-Tonalite-Dacite genesis and crustal growth via slab melting: Archean to modern comparisons. *Journal of Geophysical Research, Solid Earth*, *95*(B13), 21503–21521. https://doi.org/10.1029/jb095ib13p21503

Egüez, A., Gaona, M., & Albán, A. (2017). Mapa Geológico de la República del Ecuador. In *Ministerio de recursos no renovables del Ecuador, Quito-Ecuador* (Vol. 1). Geological Map. 1 000 000. Nacional de Investigación Geológico Minero Metalúrgico (INIGEMM).

Errázuriz-Henao, C., Gómez-Tuena, A., Duque-Trujillo, J., & Weber, M. (2019). The role of subducted sediments in the formation of intermediate mantle-derived magmas from the Northern Colombian Andes. *Lithos*, *336–337*, 151–168. https://doi.org/10.1016/j.lithos.2019.04.007

Feininger, T., & Bristow, C. R. (1980). Cretaceous and Paleogene geologic history of coastal Ecuador. *Geologische Rundschau*, *69*(3), 849–874. https://doi.org/10.1007/BF02104650

Francis, P. W., Moorbath, S., & Thorpe, R. S. (1977). Strontium isotope data for Recent andesites in Ecuador and North Chile. *Earth and Planetary Science Letters*, *37*(2), 197–202. https://doi.org/10.1016/0012-821X(77)90164-9

Fuller, S., Carey, S., & Nomikou, P. (2018). Distribution of fine-grained tephra from the 1650 CE submarine eruption of Kolumbo volcano, Greece. *Journal of Volcanology and Geothermal Research*, *352*, 10–25. https://doi.org/10.1016/j.jvolgeores.2018.01.004

Garrison, J. M., & Davidson, J. P. (2003). Dubious case for slab melting in the Northern volcanic zone of the Andes. *Geology*, *31*(6), 565–568. https://doi.org/10.1130/0091-7613(2003)031<0565:dcfsmi>2.0.co;2

Gazel, E., Hayes, J. L., Hoernle, K., Kelemen, P., Everson, E., Holbrook, W. S., et al. (2015). Continental crust generated in oceanic arcs. *Nature Geoscience*, *8*(4), 321–327. https://doi.org/10.1038/ngeo2392

Geist, D., Howard, K. A., & Larson, P. (1995). The generation of oceanic rhyolites by crystal fractionation: The basalt-rhyolite association at Volcán Alcedo, Galápagos Archipelago. *Journal of Petrology*, *36*(4), 965–982. https://doi.org/10.1093/petrology/36.4.965

Geist, D. J., McBirney, A. R., & Duncan, R. A. (1986). Geology and petrogenesis of lavas from San Cristobal island, Galapagos archipelago. *Geological Society of America Bulletin*, *97*(5), 555. https://doi.org/10.1130/0016-7606(1986)97<555:gapolf>2.0.co;2

Graindorge, D., Calahorrano, A., Charvis, P., Collot, J.-Y., & Bethoux, N. (2004). Deep structures of the Ecuador convergent margin and the Carnegie Ridge, possible consequence on great earthquakes recurrence interval. *Geophysical Research Letters*, *31*(4). https://doi.org/10.1029/2003GL018803

Gregory-Wodzicki, K. M. (2000). Uplift history of the central and northern Andes: A review. *Geological Society of America Bulletin*, *112*(7), 1091–1105. https://doi.org/10.1130/0016-7606(2000)112<1091:uhotca>2.3.co;2

Grimmer, F., Dupont, L., Lamy, F., Jung, G., González, C., & Wefer, G. (2018). Early Pliocene vegetation and hydrology changes in western equatorial South America. *Climate of the Past*, *14*(11), 1739–1754. https://doi.org/10.5194/cp-14-1739-2018

Gutscher, M.-A., Malavieille, J., Lallemand, S., & Collot, J.-Y. (1999). Tectonic segmentation of the North Andean margin: Impact of the Carnegie Ridge collision. *Earth and Planetary Science Letters*, *168*(3–4), 255–270. https://doi.org/10.1016/s0012-821x(99)00060-6

Gutscher, M.-A., Maury, R., Eissen, J.-P., & Bourdon, E. (2000). Can slab melting be caused by flat subduction? *Geology*, *28*(6), 535–538. https://doi.org/10.1130/0091-7613(2000)28<535:csmbcb>2.0.co;2

Hall, M. L., & Beate, B. (1991). El Volcanismo Plio-Cuaternario en los Andes del Ecuador. *Estudios de Geografia, 4. El paisaje volcanico de la Sierra Ecuatoriana*, 5–18.

Hall, M. L., & Calle, J. (1982). Geochronological control for the main tectonic-magmatic events of Ecuador. *Earth-Science Reviews*, *18*(3–4), 215–239. https://doi.org/10.1016/0012-8252(82)90038-1

Hall, M. L., & Mothes, P. A. (1997). Origin and age of the Upper Cangahua formation, Tumbaco Valley (Ecuador). Suelos volcánicos endurecidos (Quito, Ecuador, December 1996). In *Mem III Symp intern ORSTOM, Zebrowski, Claude; Quantin, Paul; Trujillo, Germán. EPN, Instituto Geofisico* (pp. 19–28).

Hall, M. L., & Mothes, P. A. (2008a). The rhyolitic–andesitic eruptive history of Cotopaxi volcano, Ecuador. *Bulletin of Volcanology*, *70*(6), 675–702. https://doi.org/10.1007/s00445-007-0161-2

Hall, M. L., & Mothes, P. A. (2008b). Quilotoa volcano — Ecuador: An overview of young dacitic volcanism in a lake-filled caldera. *Journal of Volcanology and Geothermal Research*, *176*(1), 44–55. https://doi.org/10.1016/j.jvolgeores.2008.01.025

Hall, M. L., & Mothes, P. A. (2008c). The Chacana caldera complex in Ecuador. *IOP Conference Series: Earth and Environmental Science*, *3*, 012004. https://doi.org/10.1088/1755-1307/3/1/012004

Hall, M. L., Mothes, P. A., Samaniego, P., Militzer, A., Beate, B., Ramón, P., & Robin, C. (2017). Antisana volcano: A representative andesitic volcano of the eastern cordillera of Ecuador: Petrography, chemistry, tephra and glacial stratigraphy. *Journal of South American Earth Sciences*, *73*, 50–64. https://doi.org/10.1016/j.jsames.2016.11.005

Hall, M. L., Robin, C., Beate, B., Mothes, P. A., & Monzier, M. (1999). Tungurahua Volcano, Ecuador: Structure, eruptive history and hazards. *Journal of Volcanology and Geothermal Research*, *91*, 1–21. https://doi.org/10.1016/s0377-0273(99)00047-5

Hall, M. L., Samaniego, P., Le Pennec, J. L., & Johnson, J. B. (2008). Ecuadorian Andes volcanism: A review of late Pliocene to present activity. *Journal of Volcanology and Geothermal Research*, *176*, 1–6. https://doi.org/10.1016/j.jvolgeores.2008.06.012

Hall, M. L., & Wood, C. A. (1985). Volcano-tectonic segmentation of the northern Andes. *Geology*, *13*(3), 203–207. https://doi.org/10.1130/0091-7613(1985)13<203:vsotna>2.0.co;2

Harmon, R. S., Barreiro, B. A., Moorbath, S., Hoefs, J., Francis, P. W., Thorpe, R. S., et al. (1984). Regional O-Sr-and Pb-isotope relationships in late Cenozoic calc-alkaline lavas of the Andean Cordillera. *Journal of the Geological Society*, *141*(5), 803–822. https://doi.org/10.1144/gsjgs.141.5.0803

Harpp, K. S., Geist, D. J., Koleszar, A. M., Christensen, B., Lyons, J., Sabga, M., & Rollins, N. (2014). The geology and geochemistry of Isla Floreana, Galápagos: A different type of late-stage ocean island volcanism. In K. S. Harpp, E. Mittelstaedt, N. d'Ozouville, & D. W. Graham (Eds.), *Geophysical Monograph series* (pp. 71–117). John Wiley & Sons, Inc. https://doi.org/10.1002/9781118852538.ch6

Harpp, K. S., Wanless, V. D., Otto, R. H., Hoernle, K., & Werner, R. (2005). The Cocos and Carnegie aseismic ridges: A trace element record of long-term plume - Spreading center interaction. *Journal of Petrology*, *46*(1), 109–133. https://doi.org/10.1093/petrology/egh064

Hernández, M. J., Michaud, F., Collot, J.-Y., d'Acremont, E., Proust, J.-N., & Barba, D. (2024). Evolution of the Manabí forearc basin in Ecuador: From the collision of Caribbean oceanic plateau to the build up of the Andes and Coastal Cordilleras. *Tectonophysics*, *870*, 230133. https://doi.org/10.1016/j.tecto.2023.230133

Hey, R. (1977). Tectonic evolution of the Cocos-Nazca spreading center. *Geological Society of America Bulletin*, *88*(10), 1404–1420. https://doi.org/10.1130/0016-7606(1977)88<1404:teotcs>2.0.co;2

Hidalgo, S. (2006). *Les interactions entre magmas calco-alcalins "classiques" et adakitiques: exemple du complexe volcanique Atacazo-Ninahuilca (Equateur)* (PhD Thesis). Université Blaise Pascal-Clermont-Ferrand II, France.

Hidalgo, S., Gerbe, M. C., Martin, H., Samaniego, P., & Bourdon, E. (2012). Role of crustal and slab components in the Northern Volcanic Zone of the Andes (Ecuador) constrained by Sr–Nd–O isotopes. *Lithos*, *132–133*, 180–192. https://doi.org/10.1016/j.lithos.2011.11.019

Hidalgo, S., Monzier, M., Almeida, E., Chazot, G., Eissen, J.-P., van der Plicht, J., & Hall, M. L. (2008). Late Pleistocene and Holocene activity of the Atacazo–Ninahuilca volcanic complex (Ecuador). *Journal of Volcanology and Geothermal Research*, *176*(1), 16–26. https://doi.org/10.1016/j.jvolgeores.2008.05.017

Hidalgo, S., Monzier, M., Martin, H., Chazot, G., Eissen, J.-P., & Cotten, J. (2007). Adakitic magmas in the Ecuadorian volcanic front: Petrogenesis of the Iliniza volcanic complex (Ecuador). *Journal of Volcanology and Geothermal Research*, *159*(4), 366–392. https://doi.org/10.1016/j.jvolgeores.2006.07.007

Hoernle, K., Werner, R., Phipps Morgan, J., Garbe-Schönberg, D., Bryce, J., & Mrazek, J. (2000). Existence of complex spatial zonation in the Galápagos plume. *Geology*, *28*(5), 435–438. https://doi.org/10.1130/0091-7613(2000)028<0435:eocszi>2.3.co;2

Hoffer, G. (2008). *Fusion partielle d'un manteau métasomatisé par un liquide adakitique: approches géochimique et expérimentale de la genèse et de l'évolution des magmas de l'arrière-arc équatorien* (PhD Thesis). Université Blaise Pascal-Clermont-Ferrand II, France.

Hoffer, G., Eissen, J.-P., Beate, B., Bourdon, E., Fornari, M., & Cotten, J. (2008). Geochemical and petrological constraints on rear-arc magma genesis processes in Ecuador: The Puyo cones and Mera lavas volcanic formations. *Journal of Volcanology and Geothermal Research*, *176*(1), 107–118. https://doi.org/10.1016/j.jvolgeores.2008.05.023

Hollister, V. F., & Sirvas, E. B. (1978). The Calipuy formation of northern Peru, and its relation to volcanism in the northern Andes. *Journal of Volcanology and Geothermal Research*, *4*(1–2), 89–98. https://doi.org/10.1016/0377-0273(78)90030-6

Hungerbühler, D., Steinmann, M., Winkler, W., Seward, D., Egüez, A., Peterson, D. E., et al. (2002). Neogene stratigraphy and Andean geodynamics of southern Ecuador. *Earth-Science Reviews*, *57*(1–2), 75–124. https://doi.org/10.1016/S0012-8252(01)00071-X

James, D. E., & Murcia, L. A. (1984). Crustal contamination in northern Andean volcanics. *Journal of the Geological Society*, *141*(5), 823–830. https://doi.org/10.1144/gsjgs.141.5.0823

Jaramillo, J. S., Cardona, A., Monsalve, G., Valencia, V., & León, S. (2019). Petrogenesis of the late Miocene Combia volcanic complex, northwestern Colombian Andes: Tectonic implication of short term and compositionally heterogeneous arc magmatism. *Lithos*, *330–331*, 194–210. https://doi.org/10.1016/j.lithos.2019.02.017

Laeger, K., Halama, R., Hansteen, T., Savov, I. P., Murcia, H. F., Cortés, G. P., & Garbe-Schönberg, D. (2013). Crystallization conditions and petrogenesis of the lava dome from the ~900 years BP eruption of Cerro Machín Volcano, Colombia. *Journal of South American Earth Sciences*, *48*, 193–208. https://doi.org/10.1016/j.jsames.2013.09.009

Lavenu, A., Noblet, C., Bonhomme, M. G., Egüez, A., Dugas, F., & Vivier, G. (1992). New K-Ar age dates of Neogene and Quaternary volcanic rocks from the Ecuadorian Andes: Implications for the relationship between sedimentation, volcanism, and tectonics. *Journal of South American Earth Sciences*, *5*(3–4), 309–320. https://doi.org/10.1016/0895-9811(92)90028-w

Lavenu, A., Winter, T., & Dávila, F. (1995). A Pliocene–Quaternary compressional basin in the Interandean Depression, Central Ecuador. *Geophysical Journal International*, *121*, 279–300. https://doi.org/10.1111/j.1365-246X.1995.tb03527.x

Legros, F. (2000). Minimum volume of a tephra fallout deposit estimated from a single isopach. *Journal of Volcanology and Geothermal Research*, *96*(1–2), 25–32. https://doi.org/10.1016/S0377-0273(99)00135-3

Le Pennec, J.-L., De Saulieu, G., Samaniego, P., Jaya, D., & Gailler, L. (2013). A devastating Plinian eruption at Tungurahua volcano reveals formative occupation at ~1100 cal BC in Central Ecuador. *Radiocarbon*, *55*(3), 1199–1214. https://doi.org/10.1017/s0033822200048116

Le Pennec, J. L., Ruiz, A. G., Eissen, J. P., Hall, M. L., & Fornari, M. (2011). Identifying potentially active volcanoes in the Andes: Radiometric evidence for late Pleistocene-early Holocene eruptions at Volcán Imbabura, Ecuador. *Journal of Volcanology and Geothermal Research*, *206*(3–4), 121–135. https://doi.org/10.1016/j.jvolgeores.2011.06.002

Lonsdale, P. (1977). Inflow of bottom water to the Panama Basin. *Deep-Sea Research*, *24*(12), 1065–1101. https://doi.org/10.1016/0146-6291(77)90514-8

Lonsdale, P. (1978). Ecuadorian subduction system. *Bulletin*, *62*. https://doi.org/10.1306/C1EA5526-16C9-11D7-8645000102C1865D

Lonsdale, P. (2005). Creation of the Cocos and Nazca plates by fission of the Farallon plate. *Tectonophysics*, *404*(3–4), 237–264. https://doi.org/10.1016/j.tecto.2005.05.011

Macdonald, R., Smith, R. L., & Thomas, J. E. (1992). *Chemistry of the subalkalic silicic obsidians* (Vol. 1523, p. 214). U.S. Geological Survey Professional Paper. Retrieved from https://pubs.usgs.gov/pp/1523/

Mamani, M., Tassara, A., & Wörner, G. (2008). Composition and structural control of crustal domains in the central Andes. *Geochemistry, Geophysics, Geosystems*, *9*, Q03006. https://doi.org/10.1029/2007GC001925

Margirier, A., Strecker, M. R., Reiners, P. W., Thomson, S. N., Casado, I., George, S. W. M., & Alvarado, A. (2023). Late miocene exhumation of the western cordillera, Ecuador, driven by increased coupling between the subducting Carnegie Ridge and the South American continent. *Tectonics*, *42*(1), e2022TC007344. https://doi.org/10.1029/2022TC007344

Martin, H., Smithies, R. H., Rapp, R., Moyen, J.-F., & Champion, D. (2005). An overview of adakite, tonalite–trondhjemite–granodiorite (TTG), and sanukitoid: Relationships and some implications for crustal evolution. *Lithos*, *79*(1–2), 1–24. https://doi.org/10.1016/j.lithos.2004.04.048

Melson, W. G., Allan, J. F., Jerez, D. R., Nelen, J., Calvache, M. L., Williams, S. N., et al. (1990). Water contents, temperatures and diversity of the magmas of the catastrophic eruption of Nevado del Ruiz, Colombia, November 13, 1985. *Journal of Volcanology and Geothermal Research*, *41*(1–4), 97–126. https://doi.org/10.1016/0377-0273(90)90085-T

Meschede, M., & Barckhausen, U. (2001). The relationship of the Cocos and Carnegie ridges: Age constraints from paleogeographic reconstructions. *International Journal of Earth Sciences*, *90*(2), 386–392. https://doi.org/10.1007/s005310000155

Michaud, F., Collot, J. Y., Ratzov, G., Proust, J. N., Dano, A., Lebrun, J. F., et al. (2018). A honeycomb seafloor morphology in carbonate sediment of the Carnegie Ridge (offshore Ecuador): Formation and potential geodynamic significance. *Geology*, *46*(11), 979–982. https://doi.org/10.1130/G45285.1

Michaud, F., Witt, C., & Royer, J.-Y. (2009). Influence of the subduction of the Carnegie volcanic ridge on Ecuadorian geology: Reality and fiction. *Geological Society of America Memoir*, *204*(10), 217–228. https://doi.org/10.1130/2009.1204

Monsalve, M. L., Ortiz, I. D., & Norini, G. (2019). El Escondido, a newly identified silicic Quaternary volcano in the NE region of the northern volcanic segment (Central Cordillera of Colombia). *Journal of Volcanology and Geothermal Research*, *383*, 47–62. https://doi.org/10.1016/j.jvolgeores.2017.12.010

Monzier, M., Robin, C., Samaniego, P., Hall, M. L., Cotten, J., Mothes, P., & Arnaud, N. (1999). Sanguay volcano, Ecuador: Structural development, present activity and petrology. *Journal of Volcanology and Geothermal Research*, *90*(1–2), 49–79. https://doi.org/10.1016/s0377-0273(99)00021-9

Moreno-Alfonso, S. C., Sánchez, J. J., & Murcia, H. (2021). Evidences of an unknown debris avalanche event (<0.58 Ma), in the active Azufral volcano (Nariño, Colombia). *Journal of South American Earth Sciences*, *107*, 103138. https://doi.org/10.1016/j.jsames.2020.103138

Mothes, P. A., & Hall, M. L. (2008). The plinian fallout associated with Quilotoa's 800 yr BP eruption, Ecuadorian Andes. *Journal of Volcanology and Geothermal Research*, *176*(1), 56–69. https://doi.org/10.1016/j.jvolgeores.2008.05.018

Murcia, H. F., Hurtado, B. O., Cortés, G. P., Macías, J. L., & Cepeda, H. (2008). The ~2500 yr B.P. Chicoral non-cohesive debris flow from Cerro Machín Volcano, Colombia. *Journal of Volcanology and Geothermal Research*, *171*, 201–214. https://doi.org/10.1016/j.jvolgeores.2007.11.016

Narváez, D. F., Samaniego, P., Koga, K. T., Rose-Koga, E. F., Hidalgo, S., & Ratzov, G. (2023). Two types of slab components under Ecuadorian volcanoes supported by primitive olivine-hosted melt inclusion study. *Lithos*, *442–443*, 107049. https://doi.org/10.1016/j.lithos.2023.107049

Ninkovich, D., & Shackleton, N. J. (1975). Distribution, stratigraphic position and age of ash layer "L". *Panama Basin region. Earth and Planetary Science Letters*, *27*(1), 20–34. https://doi.org/10.1016/0012-821x(75)90156-9

Nocquet, J.-M., Villegas-Lanza, J. C., Chlieh, M., Mothes, P. A., Rolandone, F., Jarrin, P., et al. (2014). Motion of continental slivers and creeping subduction in the northern Andes. *Nature Geoscience*, *7*(4), 287–291. https://doi.org/10.1038/ngeo2099

Opdyke, N. D., Hall, M., Mejia, V., Huang, K., & Foster, D. A. (2006). Time-averaged field at the equator: Results from Ecuador. *Geochemistry, Geophysics, Geosystems*, *7*(11). https://doi.org/10.1029/2005GC001221

Paquereau-Lebti, P., Thouret, J.-C., Wörner, G., & Fornari, M. (2006). Neogene and Quaternary ignimbrites in the area of Arequipa, southern Peru: Stratigraphical and petrological correlations. *Journal of Volcanology and Geothermal Research*, *154*(3–4), 251–275. https://doi.org/10.1016/j.jvolgeores.2006.02.014

Pardo, N., Sulpizio, R., Lucchi, F., Giordano, G., Cronin, S., Pulgarín, B. A., et al. (2023). Late Holocene volcanic stratigraphy and eruption chronology of the dacitic Young Doña Juana volcano, Colombia. *GSA Bulletin*. https://doi.org/10.1130/B36557.1

Peccerillo, A., & Taylor, S. R. (1976). Geochemistry of Eocene calc-alkaline volcanic rocks from the Kastamonu area, northern Turkey. *Contributions to Mineralogy and Petrology*, *58*(1), 63–81. https://doi.org/10.1007/bf00384745

Pedoja, K., Dumont, J. F., Lamothe, M., Ortlieb, L., Collot, J.-Y., Ghaleb, B., et al. (2006). Plio-quaternary uplift of the Manta Peninsula and La Plata island and the subduction of the Carnegie Ridge, central coast of Ecuador. *Journal of South American Earth Sciences*, *22*(1–2), 1–21. https://doi.org/10.1016/j.jsames.2006.08.003

Petford, N., & Atherton, M. P. (1994). Cretaceous-Tertiary volcanism and syn-subduction crustal extension in northern central Peru. *Science Progress*, *81*(1), 233–248. https://doi.org/10.1144/GSL.SP.1994.081.01.13

Pouclet, A., Cambray, H., Cadet, J.-P., Bourgeois, J., & De Wever, P. (1990). Proceedings of the ocean drilling program. *112 Scientific Reports*. https://doi.org/10.2973/odp.proc.sr.112.1990

Prival, J.-M., Thouret, J.-C., Japura, S., Gurioli, L., Bonadonna, C., Mariño, J., & Cueva, K. (2020). New insights into eruption source parameters of the 1600 CE Huaynaputina Plinian eruption, Peru. *Bulletin of Volcanology*, *82*(1), 7. https://doi.org/10.1007/s00445-019-1340-7

Ramon, P., Vallejo, S., Mothes, P., Andrade, D., Vásconez, F., Yepes, H., et al. (2021). Instituto Geofísico - Escuela Politécnica Nacional, the Ecuadorian seismology and volcanology service. *Volcanica*, *4*(S1), 93–112. https://doi.org/10.30909/vol.04.S1.93112

Reyes, P. (2013). *Evolution du relief le long des marges actives: étude de la déformation Plio-Quaternaire de la cordillère côtière d'Equateur* (PhD Thesis). Université Nice Sophia Antipolis.

Rivera, M., Monge, R., & Navarro, P. (2005). Characterisation of the Cenozoic volcanism in northern Peru (7°45′–9°00's; 78°00′–78°45′w). Presented at the 6th International Symposium on Andean Geodynamics (ISAG), Barcelona, Spain. Extended Abstracts: 600-603.

Robin, C., Eissen, J.-P., Samaniego, P., Martin, H., Hall, M., & Cotten, J. (2009). Evolution of the late Pleistocene Mojanda–Fuya Fuya volcanic complex (Ecuador), by progressive adakitic involvement in mantle magma sources. *Bulletin of Volcanology*, *71*(3), 233–258. https://doi.org/10.1007/s00445-008-0219-9

Robin, C., Samaniego, P., Le Pennec, J.-L., Fornari, M., Mothes, P., & van der Plicht, J. (2010). New radiometric and petrological constraints on the evolution of the Pichincha volcanic complex (Ecuador). *Bulletin of Volcanology*, *72*(9), 1109–1129. https://doi.org/10.1007/s00445-010-0389-0

Ruprecht, P., & Plank, T. (2013). Feeding andesitic eruptions with a high-speed connection from the mantle. *Nature*, *500*(7460), 68–72. https://doi.org/10.1038/nature12342

Sallarès, V., & Charvis, P. (2003). Crustal thickness constraints on the geodynamic evolution of the Galapagos Volcanic Province. *Earth and Planetary Science Letters*, *214*(3–4), 545–559. https://doi.org/10.1016/S0012-821X(03)00373-X

Samaniego, P., Barba, D., Robin, C., Fornari, M., & Bernard, B. (2012). Eruptive history of Chimborazo volcano (Ecuador): A large, ice-capped and hazardous compound volcano in the northern Andes. *Journal of Volcanology and Geothermal Research*, *221–222*, 33–51. https://doi.org/10.1016/j.jvolgeores.2012.01.014

Samaniego, P., Martin, H., Monzier, M., Robin, C., Fornari, M., Eissen, J.-P., & Cotten, J. (2005). Temporal evolution of magmatism in the northern volcanic zone of the Andes: The geology and petrology of Cayambe volcanic complex (Ecuador). *Journal of Petrology*, *46*(11), 2225–2252. https://doi.org/10.1093/petrology/egi053

Samaniego, P., Martin, H., Robin, C., & Monzier, M. (2002). Transition from calc-alkalic to adakitic magmatism at Cayambe volcano, Ecuador: Insights into slab melts and mantle wedge interactions. *Geology*, *30*(11), 967–970. https://doi.org/10.1130/0091-7613(2002)030<0967:tfcata>2.0.co;2

Samaniego, P., Monzier, M., Robin, C., & Hall, M. L. (1998). Late Holocene eruptive activity at Nevado Cayambe volcano, Ecuador. *Bulletin of Volcanology*, *59*(7), 451–459. https://doi.org/10.1007/s004450050203

Samaniego, P., Ordóñez, J., Bablon, M., Hall, M. L., Quidelleur, X., Lahitte, P., et al. (2022). The eruptive chronology of the Carihuairazo volcano (Ecuador): Recurrent sector collapses of a Middle Pleistocene stratovolcano of the northern Andes. *Journal of South American Earth Sciences*, *116*, 103865. https://doi.org/10.1016/j.jsames.2022.103865

Samaniego, P., Robin, C., Chazot, G., Bourdon, E., & Cotten, J. (2010). Evolving metasomatic agent in the Northern Andean subduction zone, deduced from magma composition of the long-lived Pichincha volcanic complex (Ecuador). *Contributions to Mineralogy and Petrology*, *160*(2), 239–260. https://doi.org/10.1007/s00410-009-0475-5

Santamaría, S., Bablon, M., Quidelleur, X., Samaniego, P., Le Pennec, J.-L., Hidalgo, S., & Liorzou, C. (2024). Blossoming of the Pleistocene volcanism in the Ecuadorian Andes: A review based on new and recent geochronological data. *Bulletin of Volcanology*, *86*(9), 80. https://doi.org/10.1007/s00445-024-01767-z

Santamaría, S., Quidelleur, X., Hidalgo, S., Samaniego, P., Le Pennec, J.-L., Liorzou, C., et al. (2022). Geochronological evolution of the potentially active Iliniza Volcano (Ecuador) based on new K-Ar ages. *Journal of Volcanology and Geothermal Research*, *424*, 107489. https://doi.org/10.1016/j.jvolgeores.2022.107489

Santamaría, S., Quidelleur, X., Samaniego, P., Audin, L., Le Pennec, J.-L., Hidalgo, S., et al. (2023). Timing of Quaternary volcanism and its relationship with tectonics in the central segment of the Ecuadorian Andes. *Journal of Volcanology and Geothermal Research*, *442*, 107895. https://doi.org/10.1016/j.jvolgeores.2023.107895

Santamaría, S., Telenchana, E., Bernard, B., Hidalgo, S., Beate, B., Córdova, M., & Narváez, D. (2017). *Registro de erupciones ocurridas en los Andes del Norte durante el Holoceno: Nuevos resultados obtenidos en la turbera de Potrerillos* (Vol. 39, p. 9). Complejo Volcánico Chiles-Cerro Negro.

Santamaría Freire, S. (2021). *Reconstruction of the eruptive history of central Ecuador volcanoes: Constraints on the spatio-temporal evolution of the andean volcanism* (PhD Thesis). Université Paris-Sud, France.

Schindlbeck, J. C., Kutterolf, S., Freundt, A., Straub, S. M., Wang, K.-L., Jegen, M., et al. (2015). The miocene Galápagos ash layer record of integrated Ocean drilling program Legs 334 and 344: Ocean-island explosive volcanism during plume-ridge interaction. *Geology*, *43*(7), 599–602. https://doi.org/10.1130/G36645.1

Schütte, P. (2009). *Geochronology, geochemistry, and isotopic composition (Sr, Nd, Pb) of Tertiary porphyry systems in Ecuador* (PhD Thesis). Université de Genève.

Schütte, P., Chiaradia, M., & Beate, B. (2010a). Geodynamic controls on Tertiary arc magmatism in Ecuador: Constraints from U–Pb zircon geochronology of Oligocene–Miocene intrusions and regional age distribution trends. *Tectonophysics*, *489*(1–4), 159–176. https://doi.org/10.1016/j.tecto.2010.04.015

Schütte, P., Chiaradia, M., & Beate, B. (2010b). Petrogenetic evolution of arc magmatism associated with Late Oligocene to Late Miocene porphyry-related ore deposits in Ecuador. *Economic Geology*, *105*(7), 1243–1270. https://doi.org/10.2113/econgeo.105.7.1243

Shipboard Scientific Party. (1983). Sites 501, 504 and 505. In J. R. Cann, M. G. Langseth, J. Honnorez, R. P. Von Herzen, S. M. White, et al. (Eds.), *Deep-sea drilling program, initial reports* (Vol. 69). https://doi.org/10.2973/dsdp.proc.69.102.1983

Shipboard Scientific Party. (1988). Sites 504, 677 and 678. In K. Becker, H. Sakai, et al. (Eds.), *Proceedings of ocean drilling program, initial reports* (Vol. 111). https://doi.org/10.2973/odp.proc.ir.111.101.1988

Shipboard Scientific Party. (2003). Sites 1238, 1239 and 1240. In A. C. Mix, R. Tiedemann, P. Blum, et al. (Eds.), *Proceedings of ocean drilling program, initial reports* (Vol. 202). https://doi.org/10.2973/odp.proc.ir.202.101.2003

Sigmarsson, O., Condomines, M., Morris, J. D., & Harmon, R. S. (1990). Uranium and ^{10}Be enrichments by fluids in Andean arc magmas. *Nature*, *346*(6280), 163–165. https://doi.org/10.1038/346163a0

Sinton, C. W., Hauff, F., Hoernle, K., & Werner, R. (2018). Age progressive volcanism opposite Nazca plate motion: Insights from seamounts on the northeastern margin of the Galapagos Platform. *Lithos*, *310–311*, 342–354. https://doi.org/10.1016/j.lithos.2018.04.014

Spikings, R. A., Winkler, W., Hughes, R. A., & Handler, R. (2005). Thermochronology of allochthonous terranes in Ecuador: Unravelling the accretionary and post-accretionary history of the Northern Andes. *Tectonophysics*, *399*(1–4), 195–220. https://doi.org/10.1016/j.tecto.2004.12.023

Spikings, R. A., Winkler, W., Seward, D., & Handler, R. (2001). Along-strike variations in the thermal and tectonic response of the continental Ecuadorian Andes to the collision with heterogeneous oceanic crust. *Earth and Planetary Science Letters*, *186*(1), 57–73. https://doi.org/10.1016/s0012-821x(01)00225-4

Steph, S., Tiedemann, R., Prange, M., Groeneveld, J., Schulz, M., Timmermann, A., et al. (2010). Early Pliocene increase in thermohaline overturning: A precondition for the development of the modern equatorial Pacific cold tongue. *Paleoceanography*, *25*(2). https://doi.org/10.1029/2008PA001645

Sun, S.-s., & McDonough, W. F. (1989). Chemical and isotopic systematics of oceanic basalts: Implications for mantle composition and processes. *Geological Society, London, Special Publications*, *42*(1), 313–345. https://doi.org/10.1144/GSL.SP.1989.042.01.19

Thouret, J. C., Cantagrel, J.-M., Robin, C., Murcia, A., Salinas, R., & Cepeda, H. (1995). Quaternary eruptive history and hazard-zone model at Nevado del Tolima and Cerro Machin volcanoes, Colombia. *Journal of Volcanology and Geothermal Research*, *66*(1–4), 397–426. https://doi.org/10.1016/0377-0273(94)00073-P

Thouret, J.-C., Cantagrel, J. M., Salinas, R., & Murcia, A. (1990). Quaternary eruptive history of Nevado del Ruiz (Colombia). *Journal of Volcanology and Geothermal Research*, *41*(1–4), 225–251. https://doi.org/10.1016/0377-0273(90)90090-3

Thouret, J.-C., Jicha, B. R., Paquette, J.-L., & Cubukcu, E. H. (2016). A 25 Myr chronostratigraphy of ignimbrites in South Peru: Implications for the volcanic history of the central Andes. *Journal of the Geological Society*, *173*(5), 734–756. https://doi.org/10.1144/jgs2015-162

Thouret, J.-C., Wörner, G., Gunnell, Y., Singer, B., Zhang, X., & Souriot, T. (2007). Geochronologic and stratigraphic constraints on canyon incision and Miocene uplift of the Central Andes in Peru. *Earth and Planetary Science Letters*, *263*(3–4), 151–166. https://doi.org/10.1016/j.epsl.2007.07.023

Torres Hernández, M. P. (2010). *Petrografía, Geocronología y Geoquímica de las Ignimbritas de la Formación Popayán, en el Contexto del Vulcanismo del Suroccidente de Colombia* (PhD Thesis). Universidad EAFIT, Departamiento de geología, Medellín, Colombia.

Turner, S. P., George, R. M. M., Evans, P. J., Hawkesworth, C. J., & Zellmer, G. F. (2000). Time-scales of magma formation, ascent and storage beneath subduction-zone volcanoes. *Philosophical Transactions of the Royal Society of London,Series A: Mathematical, Physical and Engineering Sciences*, *358*(1770), 1443–1464. https://doi.org/10.1098/rsta.2000.0598

Vallejo, C., Spikings, R. A., Horton, B. K., Luzieux, L., Romero, C., Winkler, W., & Thomsen, T. B. (2019). Late cretaceous to miocene stratigraphy and provenance of the coastal forearc and Western Cordillera of Ecuador: Evidence for accretion of a single oceanic plateau fragment. In *Andean tectonics* (pp. 209–236). Elsevier. https://doi.org/10.1016/B978-0-12-816009-1.00010-1

Vallejo Vargas, S. (2011). *Distribución de las cenizas volcánicas holocénicas - tardías en la Costa del Ecuador* (Engineer Thesis). Escuela Politécnica Nacional.

Van der Wiel, A. M. (1991). *Uplift and volcanism of the SE Colombian Andes in relation to Neogene sedimentation in the Upper Magdalena valley* (PhD Thesis). Wageningen University.

Vatin-Perignon, N., Poupeau, G., Oliver, R. A., Lavenu, A., Labrin, E., Keller, F., & Bellot-Gurlet, L. (1996). Trace and rare-earth element characteristics of acidic tuffs from Southern Peru and Northern Bolivia and a fission-track age for the Sillar of Arequipa. *Journal of South American Earth Sciences*, *9*(1–2), 91–109. https://doi.org/10.1016/0895-9811(96)00030-2

Villagómez, D., & Spikings, R. (2013). Thermochronology and tectonics of the central and western cordilleras of Colombia: Early cretaceous–Tertiary evolution of the northern Andes. *Lithos*, *160–161*, 228–249. https://doi.org/10.1016/j.lithos.2012.12.008

Vlastélic, I., Sainlot, N., Samaniego, P., Bernard, B., Nauret, F., Hidalgo, S., et al. (2023). Arc volcano activity driven by small-scale metasomatism of the magma source. *Nature Geoscience*, *16*(4), 363–370. https://doi.org/10.1038/s41561-023-01143-0

Wagner, L. S., Jaramillo, J. S., Ramírez-Hoyos, L. F., Monsalve, G., Cardona, A., & Becker, T. W. (2017). Transient slab flattening beneath Colombia. *Geophysical Research Letters*, *44*(13), 6616–6623. https://doi.org/10.1002/2017GL073981

Weller, D. J., Miranda, C. G., Moreno, P. I., Villa-Martínez, R., & Stern, C. R. (2015). Tephrochronology of the southernmost Andean southern volcanic zone, Chile. *Bulletin of Volcanology*, *77*(12), 107. https://doi.org/10.1007/s00445-015-0991-2

White, W. M., McBirney, A. R., & Duncan, R. A. (1993). Petrology and geochemistry of the Galapagos Islands: Portait of a pathological mantle plume. *Journal of Geophysical Research*, *98*(B11), 19533–19563. https://doi.org/10.1029/93jb02018

Williams, M., Bursik, M. I., Cortes, G. P., & Garcia, A. M. (2017). Correlation of eruptive products, Volcán Azufral, Colombia: Implications for rapid emplacement of domes and pyroclastic flow units. *Journal of Volcanology and Geothermal Research*, *341*, 21–32. https://doi.org/10.1016/j.jvolgeores.2017.05.001

Witt, C., Bourgois, J., Michaud, F., Ordoñez, M., Jiménez, N., & Sosson, M. (2006). Development of the Gulf of Guayaquil (Ecuador) during the Quaternary as an effect of the North andean block tectonic escape. *Tectonics*, *25*(3). https://doi.org/10.1029/2004TC001723

Yepes, H., Audin, L., Alvarado, A., Beauval, C., Aguilar, J., Font, Y., & Cotton, F. (2016). A new view for the geodynamics of Ecuador: Implication in seismogenic source definition and seismic hazard assessment. *Tectonics*, *35*(5), 1249–1279. https://doi.org/10.1002/2015TC003941